PHASE TRANSFORMATIONS

IN THE INTERMETALLIC COMPOUND TiNi

PHASE TRANSFORMATIONS IN THE

INTERMETALLIC COMPOUND TiNi

By

DONALD PETER DAUTOVICH, B.A.

A Thesis

Submitted to the Faculty of Graduate Studies

in Partial Fulfilment of the Requirements

for the Degree

Master of Science

McMaster University

April 1965

MASTER OF SCIENCE   McMASTER UNIVERSITY
(Metallurgy)   Hamilton, Ontario

TITLE: Phase Transformations in the Intermetallic Compound TiNi.

AUTHOR: Donald Peter Dautovich, B.A.

SUPERVISOR: Dr. G. R. Purdy

NUMBER OF PAGES: ix, 39

SCOPE AND CONTENTS:

Survey work has resolved certain reported anomalies in this system.
In particular, TiNi was found to undergo two displacive phase transfor-
mations at temperatures near room temperature. Below 50°C the pseudo
body-centered cubic compound undergoes a gradual distortion in an unusual
second order phase transformation producing the "transition phase", the
existence of which is terminated by a typical martensitic burst transfor-
mation at 20°C which produces the "martensitic phase". The crystal
structures of the parent phase and transformation products, and the trans-
formation characteristics have been studied with X-ray and electron diffrac-
tion, electron microscopy, electrical resistance and density measurements.

ACKNOWLEDGMENTS

Table of Contents

List of Tables

List of Illustrations

Introduction

The unusual ductility of the intermetallic compound TiNi coupled with other promising properties (ie. moderate density, good strength, corrosion resistance and high melting point) has inspired considerable effort for its development as an engineering alloy.

Unfortunately all the past work has not been in agreement. There has been confusion concerned with the equilibrium state of TiNi at various temperatures. Some workers (2,3) reported a high temperature (600 - 800°C) eutectoid decomposition of TiNi into Ti_2Ni and $TiNi_3$ while others (4,6) could detect no evidence of this transformation. A room temperature eutectoid decomposition has been proposed (8) and subsequently retracted (9). Purdy and Parr (6) suggested the room temperature transformation was diffusionless and hence not a eutectoid decomposition.

A brief survey of the literature clearly indicated that additional work was necessary to solve the eutectoid problem. Of greater interest however was the diffusionless room temperature transformation observed by Purdy and Parr (6) and by Buehler and Wiley (7). During the course of this work, it became evident that the room temperature transformation was not one transformation, but two. The first is an unusual diffusionless transformation in which the parent phase undergoes a continuous homogeneous shear which is disrupted only when the system is strongly supercooled with respect to the second transformation product, a typical martensite.

An electron microscopic investigation revealed an interesting substructure which inspired an investigation of the crystal structure of the pseudo body-centered cubic parent phase and led to a proposal of an ordered substitutional defect structure.

Review of previous work

The crystallography of TiNi and the equilibrium diagram in the range 50%* Ni have been the subjects of several investigations. Laves and Wallbaum (1) reported TiNi as body centered cubic (A_2). Duwez and Taylor (2) found TiNi to be body centered cubic with $a_o = 2.98\text{Å}$. They (2) also reported a eutectoid decomposition of TiNi into $TiNi_3$ and Ti_2Ni after prolonged heating of sintered powder specimens at both $650^\circ C$ and $800^\circ C$ as did Poole and Hume-Rothery (3). Margolin, Ence and Nielson (4) and Purdy and Parr (6) observed no decomposition of TiNi in samples (47% and 51% Ni) quenched from above and below $800^\circ C$. Pietrokowsky and Youngkin (5) observed simple cubic super lattice diffraction maxima indicating a CsCl type ordering.

A metallographic and X-ray diffraction investigation by Purdy and Parr (6) indicated that TiNi occurred off stoichiometry at 51% Ni with a range in composition of 2.5% Ni at $800^\circ C$ and 0.4% Ni at $500^\circ C$. They (6) also discovered a transformation of TiNi to a previously unreported phase ("π") tentatively indexed it as hexagonal and indicated it was probably diffusionless.

Purdy and Parr (6) further indicated that the "π" phase transformed completely and reversibly at $36^\circ C$ in both solid and powder form in alloys containing from 34.8% to 47% Ni, while alloys from 48% to 50% Ni began transforming at $36^\circ C$ but did not go to completion. In all cases, the transformation was found to be much slower in solid samples.

- 3 -

*all percentages quoted in atomic percent

Buehler and Wiley (7) in an attempt to resolve the differences of the Ti-Ni phase diagram as reported (Fig. 7), conducted a study of the system in the region of TiNi. Using X-ray diffraction, metallography, hardness and internal friction, they found evidence that confirmed the equilibrium relationship (Fig. 7, part C) as suggested by Purdy and Parr (6), as well as the room temperature transformation of TiNi.

In contradiction to Purdy and Parr (6), and Buehler and Wiley (7), Buehler, Gilfrich and Wiley (8) report that in alloys containing less than 49% Ni, TiNi dissociates thermally and during mechanical deformation into Ti_2Ni and $TiNi_3$ with startling dimensional and vibrational damping changes, at temperatures near room temperature.

Buehler and Wang (9) have done single crystal and polycrystalline X-ray diffraction work on TiNi at various temperatures and report an order-disorder transformation between $600^{\circ}C$ and $700^{\circ}C$ (disordered $\rightleftharpoons$ CsCl ordering) followed by a transformation to a martensitic phase "$\gamma 1$" in the temperature range $20^{\circ}C - 40^{\circ}C$ (indexed as a simple cubic $a_o = 9.03\text{Å}$), and below $20^{\circ}C$ a second martensitic phase "$\gamma 2$" (tetragonal, $a = b = 9.0\text{Å}$, $c = 3.0\text{Å}$). These authors (9) further indicate that both $\gamma 1$ and $\gamma 2$ coexist with the parent phase at temperatures up to $250^{\circ}C$ (contrary to known martensitic transformations) and also that the relative X-ray intensities of the parent TiNi phase to those of $\gamma 1$ and $\gamma 2$ remain constant, suggesting that the volume ratios of these phases remain constant over the range $250^{\circ}C$ to $-20^{\circ}C$. Buehler and Wang (9) postulate the martensitic transformations to occur by "some cooperative order-disorder mechanism of the existing phase volumes" rather than by the more typical transformation of parent to daughter phase accompanied by volume changes. They also suggest that it is this cooperative coexistence that is primarily responsible for the ductility of the alloy.

Theory of diffusionless transformations

3.1 Introduction

The most common type of diffusionless phase transformation observed in metallic systems is the martensitic transformation. Since these have been most extensively investigated, their properties serve as a useful reference in the discussion of diffusionless phase transformations in general.

Although it would be helpful to define the martensitic phase transformation concisely, this is a difficult task since many features are peculiar only to certain systems. Thus by way of definition, certain of the most characteristic features will be outlined below.

Martensitic transformations are diffusionless, all atom movements being less than one atom spacing, with the result that the chemical composition before and after transformation is the same. Atom movement across the martensite-parent interface is not thermally activated (transformations have been observed at temperatures approaching absolute zero in Fe-Ni and Fe-Ni-C alloys) and can be described as cooperative and shear-like. Normally the lattice deformation is homogeneous only in localized regions with interfacial fit maintained by slip or twinning at the interface.

Since much of the early work was done on systems in which the martensite was metastable with respect to decomposition products of different compositions there has been a tendency to make this situation a criterion for martensitic transformations. More recent work has been done on systems which do not tend to decompose and yet undergo phase transformations which

Sections 3.1 through 3.14 are based largely on the review article by Kaufman and Cohen (12).

are strikingly martensitic. Indeed, martensitic transformations have been studied in single component systems (e.g. Zr) (10).

The martensitic transformation has been classified by Buerger (11) as one of a more general family of transformations called "displacive transformations". Buerger (11) points out that, in this type of transformation, the high temperature phase space network loses symmetry by systematic distortion, maintaining close coupling as it transforms to the lower temperature phase.

3.2 Types of martensitic transformations

(a) Athermal martensite

A martensitic transformation is said to be athermal if transformation occurs only during cooling. There are two main types of athermal kinetics, those associated with Fe-Ni alloys and those associated with Au-Cd alloys. As is seen in Fig. 1, Fe-Ni exhibits a much larger hysteresis loop than Au-Cd. The Fe-Ni martensite forms by rapid growth of each nucleated plate, to full size. Thus the transformation is controlled by the rate of nucleation and the size of the fully grown plates, factors requiring large degrees of supercooling in this system.

The Au-Cd martensite plates grow rapidly to a detectable size, then by a slower intermittent growth process until interference occurs. The Au-Cd martensite thus requires little supercooling since growth, not nucleation of the plates, is the controlling factor.

(b) Isothermal martensite

Isothermal transformations exhibit C-curve kinetics. The isothermal component is not usually observed, since it is either not operative or is obscured by the athermal component in most transformations. However, it has

been detected in Fe-C-Mn and Fe-Ni-Mn alloys by Kurdjumov and Maximova (12a) above Ms (the temperature at which martensite starts forming on cooling) indicating that athermal martensite is not a necessary precursor for isothermal martensite. Since martensitic reactions are very strain sensitive and autocatalytic, athermal martensite may possibly assist the formation of isothermal martensite during a time of interrupted cooling below Ms.

Both nucleation and growth have been found to be controlling factors in isothermal transformations, depending on the alloy system. In almost all instances nucleation is the controlling factor and the transformation proceeds by immediate growth of newly nucleated plates. However, Holden (12b) and Mott and Haines (12c) have observed surface upheavals expanding with time in U-Cr alloys. Prolonged growth of martensite can only take place if the driving force is increased or the restraints removed as a function of time. Since Holden (12b) observed surface tilts at room temperature (long range diffusion was not possible) he proposed that the strain energy factor opposing the transformation is progressively relieved by time dependant yielding due to twinning in the martensite product or slip in the surroundings.

   (c)   Thermoelastic martensite

Since the discussion of thermoelastic martensite requires the use of certain thermodynamic and strain energy terms which have not yet been defined, the discussion will be deferred to a later part of this thesis.

3.3   Associated Phenomena

   (a)   Stabilization

Stabilization is the term associated with the additional supercooling required to initiate a transformation once it has stopped. It may be either the parent phase or the interface that is stabilized. Stabilization may be

caused by any of the following reasons (13):

(i) An interface may lose its glissile character if the parent or product phase plastically deforms.

(ii) The net local driving force is reduced by migration of solute atoms to the vicinity of the interface.

(iii) Dislocations in the parent phase have been pinned by solute atoms and so can no longer move to accomodate the shape change.

(b) Autocatalysis

Autocatalysis can greatly affect martensitic transformations. The stressed areas around existing plates act as preferential nucleation sites and in the extreme, a chain reaction may develop consuming the remainder of the untransformed material.

3.4 Thermodynamic considerations (12)

Chemical free energies and T_0

At the temperature T_0, the chemical free energies of the parent and martensitic phases are equal and can be expressed as

$$F^{\gamma} = F^{\alpha'} \qquad\qquad 3.1$$

where $F^{\gamma} \equiv$ free energy per mol of parent phase (termed austenite for convenience)

$F^{\alpha'} \equiv$ free energy of martensitic phase.

Their difference may be expressed as

$$F^{\gamma} - F^{\alpha'} = \Delta F^{\alpha' \to \gamma} \quad \text{cal/mol} \qquad 3.2$$

where $\Delta F^{\alpha' \to \gamma}$ is positive when martensite is more stable and negative when austenite is more stable. F^{γ} and $F^{\alpha'}$ as functions of temperature are schematically represented in Fig. 2. It should be noted from Fig. 2 that Ms and As (austenite start temperature on heating) are somewhat removed from T_0.

This hysteresis effect is due to contribution by non-chemical free energy terms which often can be minimized by introducing strain energy by plastic deformation. This yields Md (the highest temperature at which the austenite to martensite reaction is induced by plastic deformation) and Ad (the lowest temperature at which the martensite to austenite reaction is induced by plastic deformation).

3.5 Non chemical free energy terms

Martensitic transformations have always been observed to require some degree of supercooling. Although chemical free energies favour transformation at temperatures $T \; T_0$, a buildup of chemical free energy (the only driving force) is necessary to counter balance the restraining non chemical free energy terms. These non chemical free energy terms are listed below.

(a) Interfacial energy

For a lenticular plate (this shape increases the total energy by the smallest amount) of radius r and semi-thickness c where $r \gg c$, the interfacial free energy is given as

$$\Delta G_s^{\gamma \rightarrow \alpha'} = 2\pi r^2 \sigma \qquad \text{cal/particle} \qquad 3.3$$

where $2\pi r^2$ is the approximate surface area of the plate and σ is the specific interfacial free energy.

(b) Mechanical free energy

This term results from the elastic strain set up in both the martensite and the surroundings due to the dilatational and shear components of the displacements involved. The dilatational component is usually insignificant and the mechanical free energy is given by

$$\Delta G_\varepsilon^{\gamma \rightarrow \alpha'} = \pi r c^2 A = \pi r^2 c \left(\frac{Ac}{r}\right) \qquad \text{cal/particle} \qquad 3.4$$

where

$\pi r^2 c$ ≡ approximate volume of the lenticular plate

$\frac{Ac}{r}$ ≡ the strain energy referred to a unit volume of martensite

A ≡ a strain energy constant

Thus the overall free energy expression can be written

$$\Delta W^{\alpha' \to \gamma} \equiv \Delta F^{\alpha' \to \gamma} + \Delta G^{\alpha' \to \gamma} \quad \text{cal/mol} \quad 3.5$$

where
$$\Delta G = \Delta G_s + \Delta G_\varepsilon \qquad 3.6$$

In this expression $\Delta F^{\alpha' \to \gamma}$ is the driving force and $\Delta G^{\alpha' \to \gamma}$ is the restraining force. Hence for the reaction to occur ($\gamma \to \alpha'$) $\Delta F^{\alpha' \to \gamma}$ must not only be greater than zero but also must be greater than some finite quantity.

A second factor influencing the degree of super cooling necessary is the nucleation problem.

3.6 Thermoelastic martensite

In thermoelastic reactions, there is a build up of elastic energy

as the reaction proceeds. If the material is heated, this elastic energy is available to immediately reverse the reaction. There exists an intimate energy balance

$$\Delta G_\varepsilon^{\gamma \to \alpha'} = \Delta F^{\alpha' \to \gamma} \qquad 3.7$$

which when disturbed by increasing ΔF (cooling) causes the martensite to grow and when disturbed by decreasing ΔF (heating) causes the martensite to shrink.

3.7 Theories of nucleation - introduction

There are numerous theories of nucleation, of which a few are of interest since they describe in a qualitative manner certain martensitic

transformations while others are theories only in name and seem quite
untenable. This latter type will not be presented in the following
discussion.

3.8 Homogeneous nucleation theory - classical concepts

The total free energy accompanying the formation of martensite is
the sum of: the chemical free energy, $\Delta F^{\gamma \longrightarrow \alpha'}$; the strain free energy
$\Delta G_{\epsilon}^{\gamma \longrightarrow \alpha'}$; and the interfacial energy, $\Delta G_{S}^{\gamma \longrightarrow \alpha'}$.

Thus

$$\Delta w^{\gamma \longrightarrow \alpha'} = \Delta F^{\gamma \longrightarrow \alpha'} \neq \Delta G_{\epsilon}^{\gamma \longrightarrow \alpha'} \neq \Delta G_{S}^{\gamma \longrightarrow \alpha'} \quad \text{cal/particle} \quad 3.8$$

For each lenticular particle schematically shown in Fig. 3 this can
be written as

$$\Delta w^{\gamma \longrightarrow \alpha'} = \pi r^2 c \Delta f^{\gamma \longrightarrow \alpha'} \neq \pi r c^2 \Lambda \neq 2\pi r^2 \quad\quad 3.9$$

$$\Delta w^{\gamma \longrightarrow \alpha'} = 2\pi r^2 \neq \pi r^2 c(\Delta f^{\gamma \longrightarrow \alpha'} \neq \Lambda c/r) \quad \text{cal/particle} \quad 3.10$$

where $\quad \Delta f^{\gamma \longrightarrow \alpha'} = \dfrac{\Delta F^{\gamma \longrightarrow \alpha'}}{V_m}$ \quad\quad 3.11

$\Delta f^{\gamma \longrightarrow \alpha'}$ is negative below T_0 while σ and Λ are positive.

The critical values of c and r are obtained by setting

$$\frac{\partial(\Delta w^{\gamma \longrightarrow \alpha'})}{\partial c} = 0 \quad\quad 3.12$$

$$\frac{\partial(\Delta w^{\gamma \longrightarrow \alpha'})}{\partial r} = 0 \quad\quad 3.13$$

Differentiation and substitution yields the following critical
values

$$c^* = \frac{-8\sigma}{3\Delta f} \text{ cm} \quad\quad\quad r^* = \frac{-2\Lambda c^*}{\Delta f} \text{ cm}$$

$$\Delta w^* = \frac{512\pi \Lambda^2 \sigma^3}{27\Delta f^4} \text{ cal/particle} \quad V^* = \pi r^{*2} c^* = \frac{-4w^*}{\Delta f} \text{ cm}^3 \quad 3.14$$

where Δw^* is the free energy of nucleation and represents the energy barrier that must be overcome for embryos to reach critical size and spontaneous growth.

Classically Δw^* is supplied only by thermal fluctuations and each atom is regarded as a potential nucleation site. Thus the rate of nucleation can be expressed by

$$\dot{N} = (\frac{No}{Vm}) \nu \quad \exp (-\frac{w^*}{kT}) \quad \text{nuclei/cm}^3 \text{ sec.} \qquad 3.15$$

where

$\frac{No}{Vm} \equiv$ the number of atoms per cm^3

$\nu \equiv$ lattice vibration frequency and is taken as the number of nucleation attempts per second about each atom.

$\exp (-\frac{w^*}{kT}) \equiv$ the successful fraction of these attempts.

3.9. Objections to Classical homogeneous nucleation theory.

(a) Although it is useful in explaining isothermal behavior, it does not explain athermal transformations.

(b) It predicts unreasonable values for the parameters involved.

(c) Experiments have shown that nucleation can be heterogeneous. There are certain local free energy variations in a matrix that cause certain areas to be preferred nucleation sites time after time on repeated cycling.

3.10 Heterogeneous nucleation

Cohen et al (12) have postulated the existence of structural heterogeneities consisting of non equilibrium lattice imperfections, internal surfaces and local strains due to accidents in crystal growth or plastic deformation. Such imperfections could act as martensite embryos, remaining intact

during austenitizing and acting as preferred sites for nucleation of marten-
site when $T < T_0$.

3.11 The reaction path model.

This interesting proposal (12) suggests that within each embryo, the
lattice passes through a succession of states creating a series of interme-
diate crystal structures. This succession of states is considered the
reaction path with a free energy barrier between the initial and final states.
In this model, activation is not achieved by fluctuations in embryo size but
by fluctuations in atomic configurations. When these configurations have
succeeded in progressing to the martensitic state, this state then propogates
through the surrounding material in a "wave-like" manner.

3.12 Models of martensite interfaces - introduction

Theoretical treatments of martensitic transformation kinetics can
most easily be conducted if the nature of the interface is known. Although
much experimental work with transmission electron microscopy has been done
on various martensitic transformations, information about interfaces is not
readily attainable, with the result that ideas about interfaces are largely
hypothetical.

3.13 Frank's model of the austenite-martensite interface

Frank 12(d) has proposed a dislocation interface for the f.c.c.⟶b.c.t.
martensitic transformation in steel. Since (in the composition considered)
the interface lies parallel to the $(225)_\gamma$ habit plane, he suggested that
close packed planes of the two phases meet along close packed rows. In con-
verting from f.c.c. to b.c.t., a macroscopic shear of 1/ 32 and a 5% dila-
tation produce the observed macroscopic shear and proper spacing between the

close packed rows, but the atomic arrangements in the close packed rows do not match properly. A heterogeneous shear produced by an array of screw dislocations lying parallel to the close packed directions, one between every sixth close-packed plane and comprizing the $(225)_\gamma$ interface, produces the proper atomic matching. The martensite plate grows by movement of the screw dislocations into the austenite.

Fig. 4 is a schematic drawing of Frank's model. Fig. 4 (a) is a close packed plane with vertical close packed rows, Fig. 4 (b) indicates the extension of the close packed rows, Fig. 4 (c) the shear which does not result in final atomic matching, Fig. 4 (d) illustrates the achievement of atomic matching by an array of screw dislocations and Fig. 4 (e) presents the array of dislocations in the $(225)_\gamma$ plane moving into the γ phase. The interface is coherent except for the dislocation on every sixth plane.

3.14   Knapp-Dehlinger treatment of the athermal transformation

Extending Frank's 12(d) analysis, Knapp and Dehlinger 12(e) considered the martensite embryo to be a thin oblate spheroid bounded by dislocation loops as shown in Fig. 5. They considered the embryo to grow in the $[1\bar{1}0]_\gamma$ and $[225]_\gamma$ directions by expansion of these dislocation loops while growth in the $[55\bar{4}]_\gamma$ direction required the creation of new loops.

The energy to expand and create these dislocation loops, and the strain energy, must be supplied by the chemical driving force. Contrary to the classical nucleation theory which indicates that growth of an embryo is possible when $\partial(\Delta w) = 0$, Knapp and Dehlinger suggest that an embryo will spontaneously grow to full size when $\Delta w = 0$, that is, when the chemical driving force exactly balances the strain energy and the energy needed to move and create dislocation loops.

For a unit volume of martensite, by dropping the $\gamma \longrightarrow \alpha'$ superscript it can be written that

$$\Delta w = \Delta f \not{} \Delta g \qquad cal/cm^3 \qquad\qquad 3.8$$

where Δf is negative below T_o and Δg is always positive and represents the sum of the strain and interfacial energies.

If $\frac{4}{3} \pi r^2 c$ is taken as the volume and $2 \pi r^2$ as the area of the embryo when r is radius and c the semi thickness, it can be shown for a unit volume of martensite that

$$\Delta g = \frac{3\sigma}{2c} \not{} \frac{Ac}{r} \qquad cal/cm^3 \qquad\qquad 3.9$$

where again

$\frac{Ac}{r} \equiv$ the strain energy referred to a unit volume of martensite

$\sigma \equiv$ the specific interfacial free energy.

For a given volume of embryo Δg can be minimized with respect to the volume and it can be shown that

$$\Delta g_{min} = \frac{5}{2} \left(\frac{\sigma A}{r} \right)^{1/2} = \frac{5\sigma}{2c} \qquad cal/cm^3 \qquad\qquad 3.10$$

and

$$c = \left(\frac{\sigma r}{A} \right)^{1/2} \qquad cm \qquad\qquad 3.11$$

The variation of Δg_{min} and the net driving force Δw with the radius of the embryo when suitable values are used for the constants is shown in Fig. 6.

Two conclusions can be drawn from Fig. 6:

(a) Since there is a monotonic decrease of Δg_{min} as r increases, the larger an embryo is, the smaller is the force opposing transformation.

(b) Once an embryo starts to grow the restraining force falls off progressively, thereby allowing spontaneous growth.

It is found that martensite plates usually grow until collision

with other plates occurs. However even when the number of nucleation sites are few and far between, Kaufman and Cohen (12) suggest that propagation can be stopped by jamming of the dislocations in the interface either through interactions with other dislocations or impurities or other defects, thereby destroying the close coupling between the two lattices.

3.15 Phenomonological theories of martensite formation

The distortions involved in martensitic transformations can be classified as "pure" and "impure" distortions. The "pure" distortion is defined as one in which there exists at least one set of orthogonal axes which are not rotated by the distortion. An "impure" distortion can be represented by a "pure" distortion followed by a rotation of the material as a rigid body.

The so-called "Bain distortion" is a pure distortion and involves (in the case of a cubic parent phase) contraction along one cube axis and expansion in all directions perpendicular to it. The "Bain distortion" is homogeneous only in local regions, macroscopic volumes contain either twinned or slipped regions.

Several workers (14,15,16) have formulated geometrical theories of crystallography of martensitic transformations which enable the calculation of: the normal to the interface plane; the direction and magnitude of the macroscopic distortions involved; and the orientation relationships. The initial and final lattice parameters are the only experimental data necessary.

All the theories are similar in that they require the selection of a plane which will permit correlation between the two lattices. However, they are different in the restrictions they place on this plane. Wechsler, Lieberman and Read (14) propose that the plane must have zero net distortion when averaged over many of the inhomogeneities while Frank uses a matching

technique (Fig. 4) in iron-carbon alloys to study the lattice correlation. Frank's technique has been extended to the prism-matching (16) technique in which volumes of material rather than planes are matched.

Generally, use of these theories involves putting the lattice correlation in suitable matrix form. Wechsler, Lieberman and Read have demonstrated the use of their theory as applied to Fe-Ni martensites (14) and to Au-Cd martensites (15), obtaining very good agreement with experimental values. In all cases (16) where theoretical and experimental results have been compared, the agreement has been very good. It is difficult to make a critical comparison of the existing theories (which differ only in the assumptions about the distortions to be allowed in the interface) with the existing data. However, Cohen (13) states that Bullough and Bilby (13(b)) have shown that the assumption of glissile surface dislocations, necessary for the rapid growth of martensite, is consistent with the assumption of the existence of a plane of zero net distortion used in certain crystallographic theories.

3.16. A classification of diffusionless transformations

Having outlined the state of understanding of martensitic transformations, it is now possible to compare these with other diffusionless transformations, about which comparatively little has been reported:

(a) Massive transformations (17)

These transformations are distinguishable from martensitic transformations by the fact that the parent and daughter phases are separated by a high energy highly mobile incoherent interface, which negates the possibility of any close coupling between the crystal structures of the two phases. The essential thermodynamic arguments of sections 3.4 through 3.8 have been applied to massive transformations in iron base systems by

Gilbert and Owen (18).

(b) Second order diffusionless transformations

According to Landau and Lifshitz (20) a transformation is defined an n'th order if the first discontinuity of the derivative of free energy with respect to temperature and pressure occurs in the n'th derivative. Almost all diffusionless transformations are first order transformations. However, Barium Titanate ($BaTiO_3$) (11) undergoes a second order transformation (cubic to tetragonal) involving a continuous shifting of atoms (as opposed to the instantaneous movement of atoms to final lattice positions usually observed in first order diffusionless transformations).

This type of transformation is unique in that a continuous series of crystal structures exists (cf. second order superlattice transformations) and in that a classical nucleation event need not precede the formation of the daughter phase (cf. diffusional spinodal decomposition reactions (19)). The second order diffusionless transformation and the martensitic transformation fit Buerger's definition of a "displacive transformation" while the massive transformation is "reconstructive".

SECTION 4

Experimental

4.1. Alloys

Ingots of 51% Ni were prepared using iodide titanium (99.92%) and standard spectrographic nickel, (99.998%), both by levitation and argon arc melting in gettered inert atmospheres. The ingots were reduced to wire and sheet form by a combination of hot and cold rolling in air. (The alloy preparation is discussed more fully in Appendix A). This alloy was studied by: optical and electron metallography; electron and X-ray diffraction; resistivity and density measurements.

Alloys of 50% Ni and 50.4% Ni in wire form were obtained from W. J. Buehler at U.S. Naval Ordnance Laboratories and were studied by X-ray diffraction without additional heat treatment.

4.2. Heat treatment

51% Ni wire (0.040 inches in diameter) and sheet (0.020 inches and 0.003 inches thick) were electropolished (Appendix B) to remove scale and contaminant diffusion zone prior to heat treatment. The samples were sealed in vycor tubing at 10^{-6}m.m. Hg and annealed at 700°C and 500°C for various times as indicated by Table 1. Material annealed in this manner always retained the bright electropolished appearance.

Other samples were heat treated at 700°C for 1200 minutes followed by 1800 minutes at 500°C (specifically to produce the martensitic phase which is discussed later) in argon atmospheres. Material annealed in this

manner occasionally had surface discolouration.

4.3. Electrical resistance

The equipment used for electrical resistance measurements consisted of: a Pye potentiometer sensitive to changes of one microvolt; a Metra d'Arsonval galvanometer; two 2 volt-200 ampere hour batteries; a 0.1 ohm Manganin wound standard resistor; a wire wound variable step resistor; and a silver contact four pole reversing switch which permitted the simultaneous reversal of the current in the main circuit and the potentiometer circuit.

(a) Parent phase

The absolute resistivity was measured in samples H-700-1,2,3,4 and H-500-1. The specimen holder was equipped to accept 0.040" wire samples. A constant gauge length was maintained by two fixed spring steel knife edged pressure contacts. A potential was placed across the specimen through lead pressure contacts. The resistance was determined by averaging the voltage drops of four current settings of approximately 0.02 amperes delivered in forward and reverse directions while the specimen was maintained at 90°C with a "Haake unitherm" temperature controller (to avoid the displacive transformations). Since absolute resistivities were desired, it was necessary to maintain reproduceable electrical contacts. Contact reproduceability was checked by mounting and dismounting sample H-700-4 to get three resistivity determinations.

(b) Displacive transformations

During the course of this work it was found that the parent phase underwent a diffusionless transformation at about 50°C to the "transition phase" followed by a second diffusionless transformation at 20°C to the "martensitic phase".

The resistance change accompanying the displacive transformations was studied in the temperature range -60°C to 120°C in 50% Ni wire (0.020" diameter) obtained from W. J. Buehler. The temperature of the specimen (contained in a rubber bladder) was controlled by a dry ice-methanol bath (-60° to 25°C) and a detergent ("Xyro L") bath heated with the "Haake unitherm" controller (25° to 120°C). The specimen temperature was determined by a thermocouple fixed about $\frac{1}{2}$ inch from the specimen. Cooling and heating rates of approximately 1° per minute permitted resistance determinations with the current flowing in one direction only. Since contact resistance was not critical in this experiment a very simple specimen holder consisting of a micarta base plate and two copper pressure contacts was used. The low temperature $\beta \longrightarrow \alpha$ transformation in tin prevented the use of lead-tin solders.

4.4. X-ray diffraction

X-ray diffraction studies were made on 50% Ni, 50.4% Ni and 51% Ni alloys using standard Debye-Scherrer techniques. Secondary fluorescence excited in the Ti by the Cuk_α radiation was absorbed by a 0.005" nickel strip placed next to the film (for diffracted Cuk_α $I/Io \doteqdot 0.5$, for secondary Tik_α $I/I \doteqdot 0.002$). Electropolished wire specimens (0.005 - 0.015 inches in diameter) were exposed for about 24 hours in the small camera and a week in the large camera.

The parent phase was exposed at room temperature as was the martensitic phase (after determining that the martensitic phase was retained at room temperature following quenching into liquid air). The transition phase was studied at 50°C, 45°C, 40°C and 23°C. The temperature was controlled by a stream of air that had passed through a copper coil immersed

in a temperature-controlled detergent bath.

In all cases where line intensities were estimated, a flat plate camera was used to check the uniformity of the Debye rings.

Two computer programs* were used in the identification of the powder patterns: (a) DESLS and (b) DESLID

(a) DESLS

The DESLS program is a Debye-Scherrer powder identification program. This program was designed to match observed θ values with calculated θ values obtained from the lattice parameter input.

(b) DESLID

The DESLID program was designed to do a least squares refinement by changing lattice parameters in order to produce the best agreement between observed and calculated θ values.

4.5. Electron microscopy and diffraction

The complexity of the X-ray powder pattern from the martensitic phase made its solution almost an impossible task. Since single crystals were not available, thin film electron diffraction techniques were used in obtaining extra data.

Obtaining reliable crystallographic data with an electron microscope has certain inherent problems:

(i) The relatively small focal length of the objective lens makes the sample height in the microscope very critical. Errors up to 5% in interplanar spacings are possible due to variation in sample heights.

...

* The computer programs and instruction in their use were kindly given by Mr. Bev Robertson.

(ii) Distortion due to the projector lens is greater for smaller interplanar spacings so that beams diffracted through larger angles do not give   reliable data.

(iii) Since electron diffraction can occur at small deviations from the Bragg angle, one can imagine the points in reciprocal space not as points but as rods. The Ewald sphere is then able to intersect rods of two non-parallel planes in reciprocal space and result in the phenomenon known as "spiking". Thus a photographic plate is able to gather information from two non-parallel planes of reciprocal space simultaneously, resulting in a rather confusing diffraction pattern.

The type of alloy and phase transformation presented other problems:

(i) The techniques for preparing thin films of TiNi had not been developed previously and developing these techniques took considerable time.

(ii) The fact that martensites are invariably twinned, complicated the analysis of electron diffraction patterns.

(iii) The martensite crystals in TiNi proved to be very small, with the result that the microscope selector aperture often selected 3 or 4 differently oriented crystals.

It was possible to produce thin films of the martensitic phase by electropolishing (appendix B), at -15°C, 0.003 inch sheet material (51 at % Ni) that had been annealed at 700°C for 1200 minutes followed by an anneal at 500°C for 1800 minutes. Although initially the martensite crystals were extremely small, it was observed that after some weeks at room temperature, certain martensite crystals had grown at the expense of others in the already prepared thin films. This event made it possible to obtain some very good single crystal electron diffraction photographs, although there was some question as to the correspondence to bulk material.

The parent phase and transition phase were studied in thin films of the material heat treated according to Table 1. Structures that are thought to be representative of the transition phase were found in alloys H-500-3 and H-500-4 while the martensitic phase was rarely found in any of this series.

4.6. Density measurements

Density measurements were made (in H-700-3 alloy) using a 2 ml. specific gravity bottle and standard water displacement techniques.

Results and discussion

5.1. The parent phase

(a) The possibility of eutectoidal decomposition

Previous conflicting reports (2,3,4,6) concerning the possibility of a eutectoidal decomposition (Ti Ni $\longrightarrow$ Ti$_2$ Ni + Ti Ni$_3$) prompted some effort in making a final conclusion. (Hanson (21) includes the eutectoidal decomposition as one of the versions of the phase diagram in the region of Ti Ni.) An electron metallographic examination of the H series of alloys indicated no evidence for such a reaction.

There are two possible explanations to account for the reports (2,3) of eutectoidal decomposition above 600°C.

(i) Selective oxidation of Ti produces a Ni rich under-layer which may cause sufficient supersaturation of Ni to precipitate isolated particles (22) of Ti Ni$_3$ containing insufficient oxygen (in solution) to change the crystal structure. This selective oxidation is illustrated by electron probe traces showing Ni and Ti concentration profiles near the surface of an oxidized wedge-sectioned single-phase (51% Ni) specimen (Fig. 8). A metallographic examination revealed an isolated precipitate beneath the oxide layer. Prior to the work of Purdy and Parr (6) it was commonly thought that the range of composition of Ti Ni included 50% Ni at all temperatures, alloys prepared for phase purity would contain an unsuspected portion of Ti$_2$ Ni. Hence X-ray diffraction studies of the commonly used heat treated powder specimens (whose high surface to volume

ratio makes them susceptible to surface oxidation) might well show diffraction maxima corresponding to Ti_2Ni and $TiNi_3$ after prolonged annealing. 50% of the information in X-ray diffraction is obtained from a layer approximately 0.0002 inches deep in metal specimens.

(ii) The powder pattern of the room temperature diffusionless transformation product discovered by Purdy and Parr[6] bears a striking resemblance to the powder pattern that would be produced by a mixture of Ti_2Ni and $TiNi_3$. Since the reports [2,3] of eutectoidal decomposition were made previous to the work of Purdy and Parr[6] and were based on X-ray diffraction studies done at room temperature, it is conceivable that the martensitic phase was misinterpreted as a mixture of eutectoidal decomposition products. In fact, this similarity in diffraction patterns led Buehlor, Gilfrich and Wiley [8] to interpret the diffusionless transformation reported by Purdy and Parr [6] as a room temperature eutectoidal decomposition ($TiNi \longrightarrow TiNi_3 + Ti_2Ni$).

Although no evidence has been found to substantiate previous reports of a high temperature eutectoidal decomposition, it is possible to postulate a eutectoidal decomposition below $500^\circ C$ on the basis of free energy diagrams drawn to correspond to the phase diagram in Fig. 9(a). Since $TiNi$ exhibits $CsCl$ ordering [5] it is reasonable to assume that the free energy curve for $TiNi$ has a minimum at 50% Ni. The deviation from stoichiometry of $TiNi$ can be accounted for by the relatively greater thermodynamic stability of Ti_2Ni. The decreasing range in composition in the $TiNi$ phase field as the temperature is lowered suggests a eutectoidal decomposition (below $500^\circ C$) as is indicated by the free energy diagrams in Fig. 9(b).

(b) Ordering in the parent phase

Pietrokowsky and Youngkin (5), Buehler and Wang (9), and Gilfrich (23) all report Cs Cl ordering in Ti Ni. Gilfrich (23) has observed the (100) superlattice line up to 1000°C with high temperature X-ray techniques. At 650 - 700°C Gilfrich (23) reported intensity changes in the (100) and (200) diffraction maxima which he attributed to recrystallization. Buehler and Wang (9) reported an intensity change in single crystal Laue spots at this temperature, which they attributed to the Cs Cl order-disorder reaction.

The microstructure and diffraction patterns of the untransformed parent phase (51% Ni) annealed at 700°C are shown in Fig. 10(a) through Fig. 10(d). On recrystallization, the material is single phase (Fig. 10(a)) while further annealing at 700°C (times longer than 50 minutes) promotes the formation of a more complex microstructure as indicated by the striped contrast in Fig. 10(b) (discussed more fully in section 5.1(c). X-ray diffraction patterns and electron diffraction patterns taken very near the Bragg condition (Fig. 10(c) is an example) show Cs Cl superlattice maxima, in agreement with the above mentioned observations (5,9,23). However, electron diffraction patterns taken at slight deviations from the Bragg condition (Fig. 10(d)) show diffuse maxima in addition to the Cs Cl diffraction maxima. Fig. 10(d) is typical of all annealing times at 700°C.

The measured density (Table 2) of N-700-5 (6.55 ± 0.05 g/c.c.) indicates that the deviation from stoichiometry in Ti Ni is accomodated by substitutional nickel atoms in the titanium sub-lattice (calculated density for 51% Ni alloy: 6.50 ± 0.04 g/c.c.) rather than by vacant titanium sites (calculated density: 6.36 ± 0.03 g/c.c.). It should be noted that calculated densities are sensitive to the value of a_0. The limits given above

cover the range of values given in the literature for a_0

($a_0 = 3.010 \pm 0.005$ Å) (6,24,25) except that given by Duwez and Taylor (2)

($a_0 = 2.986$ Å). The possibility of Ni interstitial atoms was discarded

since this configuration was considered energetically less favourable and

X-ray diffraction patterns did not reveal the line broadening that would

accompany interstitial Ni atoms.

It is proposed that the stripe contrast of Fig. 10(b) is due to

alternate lamellae of material containing different concentrations of

ordered substitutional nickel atoms. This structure could be produced by

spinodal decomposition (section 5.1(c)).

The intensity changes noted by Buehler and Wang (9) and Gilfrich

(23) may be due to the ordering of the substitutional nickel atoms in the

lamellae of high defect concentration. However, further high temperature

X-ray studies are necessary to resolve this matter.

It may be suggested that the lamellae are anti-phase boundaries

of Cs Cl ordered domains. This idea must be discarded, however, since the

size of the ordered domains suggested by the sharply resolved $\{320\}$ and

$\{311\}$ $k_{\alpha_1} - k_{\alpha_2}$ doublets (as well as sharp lower angle superlattice lines)is not

consistent with the relatively small observed interlamellar spacing (~ 100 Å).

Subsequent annealing at 500°C promotes the Widmanstatten precipi-

tation of a second phase (initially coherent and presumed to be $Ti_2 Ni$

Fig. 11(a)).which becomes widely dispersed after long anneals. The stripe

contrast was not observed in any of the N-500 series. Electron diffraction

patterns of the N-500 series were observed to have, in addition to the

streaking (Fig. 11(b)) that is associated with the coherent precipitation

of a second phase (26), extra, sharp diffraction maxima (Fig. 11(b) and 11(c)).

The extra diffraction spots were obtainable in single phase regions between widely dispersed precipitate and are therefore associated with the parent phase. The diffraction patterns can be indexed simple cubic with unit length three times the unit length of the original Cs Cl cube. This new unit cell can be formed by substituting every third titanium atom in the cubic directions of the titanium sub-lattice by a nickel atom, thereby producing an ordered defect structure with a unit cell ($a_0 = 9.03$ Å) containing 28 nickel atoms and 26 titanium atoms (such a unit cell would result in a composition of 51.8% Ni). It was not possible to verify the existence of the 9 Å unit cell with low angle X-ray studies of super lattice reflections (with suitable Lorentz factors) due to a strong white component of the filtered Cu K_α radiation and the similarity in scattering factors for nickel and titanium. However, several very faint lines at higher angles could be indexed on the basis of a 9 Å cube as is shown in Table 4.

Electrical resistivity measurements* (Table 3) made on N-700-1,2,3,4 and N-500-1 indicated that the only significant resistivity drop ($\sim 5\%$) came after the 500°C anneal. It should be noted that the decrease in resistivity accompanied by removal of the lamellar structure overweighed the resistivity increase to be expected in the precipitation of a coherent

. . . .

* Initially it was thought that both N-700 and N-500 anneals would produce single phase alloys (according to the phase diagram after Purdy and Parr (6)). The resistivity measurements were made as an attempt to explain why N-500 alloys would undergo a diffusionless transformation while the N-700 alloys would not. Further measurements (N-500-2,3,4) were not made when N-500 alloys were found to contain a precipitate.

second phase.

Thus it is inferred from X-ray and electron diffraction observations and density measurements that the extra nickel atoms in off-stoichiometric Ti Ni, are repelled by one another and occupy "wrong" (titanium) sites in a periodic manner producing a 9 $\overset{o}{A}$ simple cubic cell. Insufficient defect concentrations may result in the segregation of the extra nickel atoms into lamellae producing alternate layers of material tending toward Cs Cl ordering and material tending toward periodic substitutional defect ordering (all layers form a part of the continuous cubic lattice network).

(c) The possibilities of spinodal decomposition

(i) High temperature spinodal decomposition

The microstructure responsible for the stripe contrast in Fig. 10(b) may have developed as the product of a spinodal decomposition. Free energy diagrams are given in Fig. 12 showing interphase relations on cooling from 900°C to 700°C. The tendency to Cs Cl ordering suggests a certain thermodynamic stability which can be associated with a minimum in the free energy curve at 50% Ni. Similarly a subsidiary minimum should occur at 51.6%, corresponding to the 9 $\overset{o}{A}$ defect structure. Fig. 12 shows the development of this minimum below 800°C and the condition for the spinodal decomposition at 700°C. Although, on the basis of these hypothetical free-energy relationships, there would be a greater decrease in free energy if Ti_2 Ni precipitated, it is proposed that the nucleation barrier is sufficient to make the spinodal decomposition the favourable reaction.

(ii) Low temperature spinodal decomposition

Thin films of samples N-500-3 and N-500-4 displayed a very diffuse cellular network in addition to the Ti_2 Ni precipitate. A preliminary

inspection of these thin films after several weeks at room temperature revealed a general increase in contrast and in many cases, an alignment of the cells as shown in Fig. 13.

It is suggested that this microstructure represents the product of a spinodal decomposition reaction* whose terminal phases are Ti Ni (~ 51.8% Ni) and the metastable "face-centered-cubic" form of Ti Ni$_3$ (this metastable phase was observed by Mihalisin (27)). The free energy diagrams corresponding to this decomposition are shown in Fig. 14.

5.2. The displacive transformations

It was discovered in the course of this investigation (and independently by Buehler and Wang (9)) that Ti Ni undergoes two diffusionless transformations near room temperature. The electrical resistance as a function of temperature plotted in Fig. 15 is typical of measurements made on 50% Ni wire**. Evidence for the existence of two transformations includes the increase and subsequent decrease in resistance at 60°C and 20°C, and the marked changes in crystal structure as indicated by the

. . . .

*The basic requirement for a spinodal decomposition reaction is that the parent and the two daughter phases lie on a continuous free energy curve. It is possible to envisage this type of behaviour in this system since a series of structures can be formed by replacing the base centering atom in the tetragonal cell bounded by (101), (10$\bar{1}$), (010) (in the Cs Cl lattice) in going from a "body-centered-cubic" Cs Cl structure to a "face-centered-cubic" Cu$_3$ Au structure.

**This wire was kindly supplied by W. J. Buehler. The heat treatment consisted of short anneal at 800°C.

superimposed powder X-ray diffraction patterns in Fig. 15. The first transformation product has been designated as the "transition phase" and the second as the "martensitic phase". Buehler and Wang (9) have denoted these phases by "γ1" and "γ2" respectively while Purdy and Parr (6) originally named the martensitic phase "η".

(a) <u>The transition phase</u>

The transition phase forms by a diffusionless transformation that involves a sequence of cumulative athermal lattice perturbations. Fig. 16 contains three of a sequence of powder patterns taken below $60^{\circ}C$ showing varying degrees of lattice distortion by line splitting of varying amounts.

The gradual change in electrical resistance at about $60^{\circ}C$ indicates that the formation of the transition phase requires very little if any supercooling since the reversion temperature for the transition phase was also found to be about $60^{\circ}C$ (i.e. $T_o = 60^{\circ}C$). Some evidence of reaction stabilization was observed on holding the sample at $25^{\circ}C$ for one hour. Further cooling of 3° was necessary to start the reaction again.

It is believed that the reaction stabilization was not due to the pinning of interfaces (distinct interfaces were never observed in the transition phase) but perhaps to a frictional effect produced by the diffusion of interstitial impurities to energetically favoured interstitial sites (similar to the Snoek effect in iron (28)) produced by the transformation distortion). It is also possible that the stabilization was due to the pinning of dislocations, within the transition phase, thereby preventing the plastic strain accompanying the transformation.

Fig. 17(a) is an electron micrograph showing a matrix of transition phase containing a Ti_2 Ni precipitate and twinned martensite. Electron diffraction patterns (of which Fig. 17(b) is typical) indicate that the regions of light and dark contrast in Fig. 17(a) correspond to regions of slightly varying orientations. The electron diffraction pattern of Fig. 17(b)* shows a slight distortion to the original cubic pattern in addition to the doubling of the "{110} cubic repeat distance" indicating the selection of a new unit of symmetry (the crystallographic planes with twice the {110} cubic distance have zero structure factor for cubic unit cells).

The X-ray diffraction pattern was indexed (without the aid of single crystal data) by computer methods and is presented in Table 5 (a more complete description of the analysis of X-ray and electron diffraction patterns is given in Appendix C). The crystal structure of the transition phase was determined to be monoclinic with parameters at $23°C$ of: $a = 4.41$ Å; $b = 3.01$ Å; $c = 4.14$ Å; $\beta = 92.3°$. The new unit cell is bounded by the (101), (10$\bar{1}$), and (010) planes of the Cs Cl structure. There is little if any volume change accompanying the formation of the transition phase.

. . . .

*Fig. 17(b) is not a single crystal pattern since a single crystal pattern would show doubling in one $\langle 110 \rangle$ direction only. The fact that doubling is seen all $\langle 110 \rangle$ directions can be accounted for by the fact that regions of equivalent orientation relations i.e. $[200]_T \parallel [110]_P$, $[200]_T \parallel [101]_P$, $[200]_T \parallel [011]_P$, are small compared to the smallest area selected for diffraction (T and P denote transition and parent phases respectively).

It is expected that both transition and martensitic phases will inherit any defect structure that was present in the parent phase before transformation. This defect structure can account for the extremely complicated electron diffraction pattern of the martensitic phase in Fig. 18(c). The X-ray diffraction patterns did not contain information about the defect structure after transformation since the scattering factors for titanium and nickel are very similar and the distortion accompanying the transformation would broaden weak superlattice lines to make them indistinguishable from the background. Consequently the crystal structures of the transition and martensitic phases have been related to a CsCl structure rather than to the more complex superlattice structure proposed for the parent phase in the 500°C annealed condition. If the defect superlattice is taken into account, the lattice constants of the transition and martensitic phase may be found by multiplying the reported axial lengths by three. However there is no reason to assume that the defect superlattice is a necessary precursor for the diffusionless transformations.

(b) The martensitic phase

At 20°C the abrupt drop in resistance shown in Fig. 15 corresponds to the onset of the martensitic transformation. Fig. 18(a) and Fig. 18(b) show a typical electron micrograph of the twinned martensitic phase coupled with indexed selected area electron diffraction patterns. Fig. 18(c) is included to demonstrate the complexity of many of the patterns obtained. It was only after the martensite thin films were stored at room temperature for two or three weeks that growth of certain martensite plates permitted simpler electron diffraction patterns such as in Fig. 18(b) to be obtained. This growth phenomenon raises the question as to the correspondence to

bulk material. However, it can be said that three axial lengths were obtained from electron diffraction patterns which permitted a consistent solution of the powder pattern. Interaxial angles were obtained by a least squares fit of the parameters to the powder pattern. The martensitic phase was found to be triclinic (a = 4.60 Å, b = 2.86 Å, c = 4.11 Å, α = 90.1°, β = 90.9°, γ = 96.7°) and was indexed as in Table 6.

Fig. 19(a) and 19(b) are electron diffraction patterns (not rotated in reproduction) taken from adjacent martensite and parent phase areas. The orientation relationship is similar to that of the parent-transition case. The strong fibre texture exhibited by rolled wire specimens permitted a macroscopic determination of the orientation relationship between the parent and martensitic phases in bulk material (this was done by matching the Debye rings on the powder patterns of the two phases). The orientation relationship found in this manner was the same as found in thin films.

The complete transformation sequence on cooling is: cubic parent phase ⟶ monoclinic transition structure ⟶ triclinic martensite. A second -order transformation mechanism, which need not involve a nucleation event, apparently allows the transition structure to form at a very low degree of supercooling (and thus to accomodate, in part, the thermodynamic driving force for the transformation). This structure persists until the system becomes strongly supercooled with respect to the low-temperature phase, which then forms as the product of a "burst" transformation.

The relatively small resistance maximum (Fig. 15) observed on heating may indicate that the martensitic phase reverts directly to the parent phase. On the other hand it is possible that the parent-martensitic interface on reversion is separated by a layer of transition phase. In an

attempt to fulfill the requirement of a plane of zero not distortion specified by the Wechsler Lieberman Read [14] crystallographic theory, the martensitic habit plane chosen in the sequence: parent phase → transition phase → martensitic phase, may prevent the reversion sequence: martensitic phase → parent phase and require a small amount of transition phase between the parent and martensitic phase volumes.

The transition phase is apparently metastable with respect to the martensitic phase since mechanical deformation below $60^{\circ}C$ transforms transition phase to martensitic phase.

It is probable that the presence of Ti_2Ni will assist the formation of the martensitic phase in two ways: by physically constraining the transition structure (Fig. 17(a)) and by providing a uniform (equilibrium) composition in the TiNi phase. This would allow a rationalization of Purdy and Parr's (6) observations that the "Ms" temperature rises with increasing amounts of Ti_2Ni in TiNi.

Since the low temperature behavior of TiNi has been discussed in some detail, it is now possible to briefly point out difficulties that may have led to misinterpretation in previous investigations.

The preferred orientation exhibited by the martensitic phase that was strain induced in wire containing no fibre texture before deformation could account for the observation of Buehler, Gilfrich and Wiley (8) that TiNi transforms to Ti_2Ni in tension and $TiNi_3$ in compression since this observation was based on diffractometer scans that would view only a small portion of each Debye ring.

Any crystal structure analysis of the displacive transformation products requires a detailed knowledge of the temperature range over which

the phase of interest exists. This information was obtained in the present work through electrical resistance measurements. Buehler and Wang (9) have apparently proceeded to gather and interpret crystallographic data from the displacive transformation products without first determining the temperature range over which they exist. The crystallographic data those authors (9) present for the ' γ1' phase (which they indexed on the basis of a 9$\overset{o}{A}$ cube) may in fact be data representing a mixture of transition and martensitic phases.

Conclusions

1. No evidence was found to support previous reports of the eutectoid decomposition TiNi → Ti$_2$Ni + TiNi$_3$ above 600°C. However, free energy diagram constructions indicate a possibility for this reaction at some temperature below 500°C.

2. The deviation from stoichiometry is accomodated by substitutional nickel atoms on titanium lattice sites. Depending on composition and thermal history, these substitutional nickel atoms can order to form a simple cubic lattice (a$_o$ = 9.03 Å).

3. The room temperature behavior of TiNi was found to be strongly influenced by composition and thermal history. In the compositions studied two diffusionless transformations were observed (at temperatures near room temperature) to form a transition phase and a martensitic phase. The transition phase which apparently forms without a nucleation event was found to be monoclinic with crystal parameters at 23°C of: a = 4.41 Å; b = 3.01 Å; c = 4.14 Å; β = 92.3° (the lattice parameters change in a continuous manner from 50°C to about 20°C). When the system is sufficiently supercooled the martensitic transformation occurs forming a triclinic product: a = 4.60 Å; b = 2.86 Å; c = 4.11 Å; α = 90.1°; β = 90.9°; γ = 96.7°; which bears the following orientation relationship with the parent phase: (010)$_M$ // (010)$_P$; (002)$_M$ // (101)$_P$.

Suggestions for future work

1. The equilibrium investigations have allowed the construction of
free energy-composition diagrams. These diagrams can be used as a basis for
further experiments:

(a) The postulate of a eutectoidal decomposition reaction below
$500^{\circ}C$ can be tested by a thin film electron microscopic examination of
suitably annealed material.

(b) If the free energy configuration (Fig. 12) depicting the
spinodal decomposition in 51% Ni alloy at $700^{\circ}C$ is correct then a 51.8%
alloy should have a stable single phase microstructure at this temperature.
The suggestion that Ti_2Ni is a stable precipitate in 51% Ni alloy at $700^{\circ}C$
(Fig. 12) can be checked by up-quenching material from the two phase region
$(500^{\circ}C)$ to $700^{\circ}C$.

(c) The postulate concerning the room temperature spinodal decompo-
sition can be tested by inspecting alloys of greater nickel concentration
(farther inside the spinodal region). If the postulate is correct, even
greater changes in microsturcture (than in Fig. 13) will be observed. In
addition, the decomposition products may be present in sufficient quantities
to permit their analysis by reliable methods such as X-ray diffraction.

2. Neutron diffraction techniques can be used to confirm the evidence
for the ordering of substitutional nickel atoms.

3. The coordinated use of electrical resistance measurements, X-ray
diffraction and cold stage electron microscopy should reveal in more detail
the effect of: the transition phase; matrix composition; and the dispersion
of a second phase (Ti_2Ni or $TiNi_3$) on the martensitic transformation.

4. Careful investigations may reveal the presence of similar pre-transformation phenomena (the transition phase) in other systems.

5. The gradual distortions involved in the formation of the transition phase make this alloy suitable for measuring the changes in elastic constants accompanying a phase transformation. Such measurements may lead to fundamental knowledge of the stability of certain metallic systems.

APPENDIX A

Alloy Preparation

The alloy samples (51 at % Ni) were prepared using iodide titanium and standard spectrographic nickel (the major impurities were Zr - 0.05% and Fe - 0.0008%, respectively), both by argon-arc melting and by levitation melting with melts of about 50 grams and 3 grams respectively. The argon-arc technique was preferred since reasonable homogeneity could be obtained by melting from the top and bottom of the alloy button alternately, and the alloy was of sufficient volume to permit easy handling during the rolling procedure. Although there is considerable magnetic stirring during the levitation process, the segregation during solidification was severe enough to remain in the material even after hot working and annealing. The arc melted alloys were large enough to permit considerably more deformation (hence homogenization) and it was possible to produce phase pure material after a combination of hot and cold rolling, followed by annealing. The phase purity was checked both by light metallography and electron thin film techniques.

The alloy was prepared in both wire and sheet form, primarily with hot rolling. Considerable cold rolling was possible when the as-cast structure was destroyed. The alloy was heated to red heat (about 700°C) in air with a methane torch prior to rolling. With some practice it was possible to make 4 or 5 passes with each heating before the alloy became prohibitively tough. It was necessary to stress relieve the material after several cold rolling passes. This was accomplished by heating the material quickly in air so that the time at red heat was only a few seconds.

Estimates indicate that the diffusion depth of interstitial impurities picked up during the hot rolling operation was insignificant compared to the amount of material removed by electropolishing prior to annealing.

APPENDIX B

Electropolishing

Electropolishing of the alloy was required both for surface removal
in preparation of specimens for heat treatment and in preparation of thin
films suitable for electron microscopy. Initially, a 5-20% perchloric
acid in acetic acid solution was used and was suitable for preparing bright
surfaces but it was not suitable for preparing thin films either by the
conventional window technique or by using the PTFE holder (designed by
Aeon Laboritories), in spite of a great deal of time spent changing con-
centration, voltage, temperature and stirring conditions.

A second electrolyte was suggested by Dr. J. McGrath (Ontario
Research Foundation). A solution of 6% perchloric, 35% ethylene glycol
and 59% methyl alcohol at -10 to -20°C with a potential of 24 volts gave
excellent results with the window technique, if the solution was stirred.
The PTFE holder again proved to be a failure, the specimen being proferen-
tially attacked away from the center, in a ring near the edge of the disc
specimen (as was the case with the perchloric-acetic solution).

Thin films were made from specimens approximately 1 cm x 2 cm x 0.005
inches. The edges were coated with microstop and stirring was done by manu-
ally waving the specimen back and forth between two stainless steel cathodes.
It was found that after 10 - 20 minutes several very good thin films could
be cut from each specimen. The thin film sections were cut with a surgical
blade then always washed in methanol and sometimes in methanol followed by
an acetone rinse. It was found that thin films could be produced from
0.020 inches material in the same manner, but with considerably more
difficulty.

APPENDIX C

Analysis of X-ray and Electron Diffraction Patterns

The analysis of the X-ray diffraction patterns proved to be very difficult and was by far the most time consuming part of this work. Useful single crystal electron diffraction data was obtained for the martensitic phase only. Fortunately the distortions leading to the transition phase were sufficiently small to permit the transition phase powder pattern to bear a strong resemblance to the cubic pattern (although many extra lines were produced). Initial attempts at the solution of the transition phase structure consisted of indexing powder pattern lines with "cubic" (hkl). Later attempts included the change of the crystal coordinate system to account for weak "non-cubic" lines.

The lack of symmetry in the crystal structure of the martensitic phase made the interpretation of electron diffraction patterns difficult and often ambiguous. Twinning and the presence of the substitutional defect structure also complicated the electron diffraction patterns. It was possible after a great deal of effort to obtain axial lengths from electron diffraction patterns which permitted the solution of the martensitic phase crystal structure.

REFERENCES

1. Laves, F., Wallbaum, H.J., Naturwiss., 1939, 27, 674.

2. Duwez, P., Taylor, J.L., Trans AIME, 1950, 188, 1173.

3. Poole, J.M., Hume-Rothery, W., J. Inst. Met., 1954, 83, 473.

4. Margolin, H., Ence, E., Nielsen, J.P., Trans AIME, 1953, 197, 243.

5. Pietrokowsky, P., Youngkin, F.G., J. Appl. Phys., 1960, 31, 1763.

6. Purdy, G.R., Parr, J. Gordon, Trans AIME, 1961, 221, 636.

7. Buehler, W.J., Wiley, R.C., Trans A.S.M., 1962, 55, 269.

8. Buehler, W.J., Gilfrich, J.V., Wiley, R.C., J. Appl. Phys., 1963,
    34, 1475.

9. Buehler, W. J., Wang, F.E., Fifth International Symposium on the
    Reactivity of Solids. To be published by Elsevier Publishing
    Company, Amsterdam.

10. Burgers, W.G., Physica, 1934, 1, 561.

11. Barrett, C.S., Structure of Metals, McGraw-Hill, 1952, 579.

12. Kaufman, L., Cohen, M., Prog. in Met. Phys., 1958, 7, 165.

12(a). Kurdjumov, G.V., Maximova, O.P., Dokl. Akad. Nauk SSSR, 1948, 61, 83.

12(b). Holden, A.N., Acta Met., 1952, 1, 617.

12(c). Mott, B.W., Haines, H.R., Rev. Metall., 1954, LI No. 9.

12(d). Frank, F.C., Acta Met., 1952, 1, 15.

12(e). Knapp, H., Dehlinger, U., Acta Met., 1956, 4, 289.

13. Cohen, M., et al, Perspectives in Materials Research, Surveys of
    Naval Science, 1963, No. 10, ACR-61, 317.

13(a). Bullough, R., Bilby, B.A., Proc. Phys. Soc., 1956, B59, 1276.

14. Wechsler, M.S., Lieberman, D.S., Read, T.A., Trans AIME, 1953, 197,
    1503.

15. Wechsler, M.S., Lieberman, D.S., Read, T.A., J. Appl. Phys., 1955,
    26, 473.

REFERENCES (continued)

16. Institute of Metals Monograph and Report Series 18, 1956, 146.

17. Massalski, T.B., Acta Met., 1958, 6, 243.

18. Gilbert, A., Owen, W.S., Acta Met., 1962, 10, 45.

19. Cahn, J.W., Acta Met., 1961, 9, 795.

20. Landau, L., Lifshitz, E., Statistical Physics, Clarendon Press, 1938, 204.

21. Hansen, M., Constitution of Binary Alloys, second edition, McGraw-Hill, 1958, 1051.

22. Kirkaldy, J.S., Fedak, D.G., Trans AIME, 1962, 224, 490.

23. Gilfrich, J.V., "X-ray Diffraction Studies on the TiNi System" Proceedings 11th Annual Conference on Applications of X-ray Analysis, Denver Research Institute, 1962 (Plenum Press Inc., New York 1963).

24. Philip, T.V., Beck, P.A., Trans AIME, 1957, 209, 1269.

25. Stüwe, H., Shimomura, Y ., Z. Metallk., 1960, 51, 180.

26. Kelly, A., Nicholson, R.B., Prog. in Mat. Science 1963, 10 No. 3, 193.

27. Mihalisin, J.R., Decker, R.F., Trans AIME, 1960, 218, 507.

28. Snoek, J., Physica, 1941, 8, 771.

TABLE 1 Heat treatment schedule

Sample name	Temperature	Time (minutes)	
H-700-1	700°C	15	
H-700-2	700°C	50	
H-700-3	700°C	500	
H-700-4	700°C	5385	
H-500-1	500°C	50	*
H-500-2	500°C	460	*
H-500-3	500°C	1680	*
H-500-4	500°C	7240	*

* preceded by 5385 minutes at 700°C

TABLE 2(a) Determination of specific gravity

bottle volume by water displacement

Run	Weight of bottle (empty) (g)	Weight of bottle (full) (g)	T (°C)	ρ_T (g/c.c.)	Volume (c.c.)
1	5.47305	7.46822	23.0	0.99756	2.00005
2	5.47290	7.46777	2210	0.99780	1.99927
3	5.47320	7.46773	24.0	0.99732	1.99989
4	5.47338	7.46912	24.0	0.99732	2.00110

average 2.00007 c.c.

As a test one determination of the bottle volume was

done by mercury displacement. The value obtained

was 2.00005 c.c.

TABLE 2(b) Density of specimen II-700-3

Run	Specimen weight (g)	Specimen volume (c.c.)	Density
1	0.35552	0.05422	6.56 g/c.c.
2	0.43417	0.06628	6.55
3	0.49591	0.07586	6.54

TABLE 5(a) Resisitivity of samples

H-700-1, 2, 3, 4 and H-500-1

measured at 90°C (gauge length 9.6825 cm)

Specimen	Cross section (cm^2)	Resistance (ohms)	Resistivity (μ-ohm-cm)
H-700-1	0.019704	0.105286	214.25
H-700-2	0.020289	0.103551	216.90
H-700-3	0.021228	0.098693	216.40
H-700-4	0.020445	0.10204	215.46
H-500-1	0.021378	0.093213	205.80

TABLE 3(b) Reproduceability of contact resistances at 90°C

Specimen H-700-4 Run 1

Rheostat Setting (Ω)	Potential drop (mV) across 0.1 standard		Potential drop (mV) across specimen		Specimen resistance (Ω)
	forward	reverse	forward	reverse	
100	2.0565	2.0582	2.1109	2.1105	0.102593
90	2.2813	2.2809	2.3408	2.3427	0.102659
80	2.5606	2.5593	2.6260	2.6289	0.102637
70	2.9168	2.9171	2.9912	2.9958	0.102590

average 0.102620

largest deviation 0.03%

Specimen H-700-4 Run 2

Rheostat setting(Ω)	Potential drop (mV) across 0.01 standard		Potential drop (mV) across specimen		Specimen resistance (Ω)
	forward	reverse	forward	reverse	
100	2.0555	2.0561	2.1058	2.1060	0.102437
90	2.2802	2.2797	2.3548	2.3354	0.102419
80	2.5583	2.5581	2.6200	2.6218	0.102451
70	2.9144	2.9147	2.9839	2.9856	0.102409

average 0.102409

largest deviation 0.04%

TABLE 3(b) (continued)

Specimen H-700-4   Run 3

Rheostat setting (Ω)	Potential drop (mV) across 0.1 standard		Potential drop (mV) across specimen		Specimen resistance (Ω)
	forward	reverse	forward	reverse	
100	2.0568	2.0569	2.0838	2.0815	0.101259
90	2.2817	2.2818	2.3059	2.3080	0.101104
80	2.5591	2.5591	2.5884	2.5882	0.101141
70	2.9167	2.9159	2.94399	2.94391	0.101084

average 0.101147

largest deviation 0.1 %

TABLE 3(c)   Summary of runs in 3(b)

Specimen H-700-4

Run	Specimen resistance (Ω)
1	0.102620
2	0.102409
3	0.101147

average 0.102055

largest deviation 0.8%

TABLE 4   Powder pattern of H-500-4

indexed on the basis of a 9.03 Å cube

Line	h k l	d (Å)	a_0 (Å)	Observed relative intensity	
1	330	2.151	9.02	vs	
2	-	2.070	-	m	*
3	633	1.229	9.04	w	
4	544,722	1.198	9.05	w	*
5	732	1.148	9.03	w	*
6	644	1.100	9.07	w	*
7	660	1.065	9.04	m	
8	662	1.042	9.04	w	*
9	900	1.009	9.08	w	
10	930	0.955	9.06	m	
11	932	0.937	9.09	w	*
12	933	0.910	9.05	w	
13	862	0.892	9.03	vw	*
14	666	0.872	9.05	m	
15	960	0.836	9.05	m	
16	963	0.807	9.06	s	

*denotes lines that do not correspond to CsCl body

centered cubic structure

TABLE 5

Observed and calculated d spacings for the transition phase at 23°C

Monoclinic   a = 4.41   b = 3.01   c = 4.14 β = 92.3°

Line	Observed d(Å)	Calculated d(Å)	h k l	Observed relative intensity
1	3.00	3.02	010	vvw
2	2.40	2.44	011	vvw
3	2.25	2.20	200	vvw
4	2.13	2.15	$\bar{1}11$	vs
5	2.10	2.11	111	vs
6	2.01	1.98	$\bar{2}01$	m
7	1.77	1.78	210	mw
8	1.50	1.50	020	m
9	1.52	1.53	212,310	vw
10	1.29	1.30	103	w
11	1.27	1.27	$\bar{3}11$	mw
12	1.24	1.24	220,311	m
13	1.22	1.22	022,$\bar{1}13$	m
14	1.16	1.17	122	w
15	1.15	1.15	203	w
16	1.12	1.13	$\bar{3}12$	mw
17	1.09	1.09	312	w
18	1.07	1.07	$\bar{2}22$	m
19	1.06	1.06	222	mo
20	1.02	1.02	$\bar{1}04,521$	m
21	0.956	0.955	$\bar{1}31$	m
22	0.948	0.950	131	m

TABLE 5 (continued)

Line	Observed d(Å)	Calculated d(Å)	h k l	Observed relative intensity
23	0.900	0.903	032	w
24	0.880	0.880	214,132,500	w
25	0.868	0.869	$\bar{5}01$	m
26	0.857	0.855	501	m
27	0.828	0.827	$\bar{4}22,330$ 005,$\bar{3}14$	mw
28	0.820	0.820	$\bar{1}05$	w
29	0.814	0.816	$\bar{3}31$	m
30	0.808	0.808	105,422	mw
31	0.803	0.803	$\bar{1}33$	s
32	0.794	0.795	133	w
33	0.789	0.792	$\bar{1}15$	w

Order of intensities   vs > s > ms > mw > w > vw > vvw

TABLE 6

Observed and calculated d spacings for the martensitic phase

Triclinic   a = 4.60   b = 2.86   c = 4.110 α = 90.1° β = 90.9°

γ = 96.7°

Line	Observed d($\overset{\circ}{A}$)	Calculated d($\overset{\circ}{A}$)	h k l	Observed relative intensity
1	4.56	4.60	100	m
2	2.81	2.86	010	w
3	2.51	2.55	$\bar{1}$10	w
4	2.34	2.33	0$\bar{1}$1,011	m
5	2.29	2.29	110,200	ms
6	2.17	2.17	$\bar{1}$11,1$\bar{1}$1	s
7	2.11	*		vw
8	2.05	2.06	002	s
9	2.00	2.00	111,$\bar{2}$01	vs
10	1.87	1.86	102	w
11	1.73	1.73	$\bar{2}$11	w
12	1.61	1.61	$\bar{1}$12	w
13	1.51	1.52	202	m
14	1.44	1.44	$\bar{3}$01	m
15	1.42	1.42	301,020	w
16	1.35	1.34	0$\bar{2}$1,$\bar{3}$11	w
17	1.29	1.29	212	w
18	1.28	1.28	310	w
19	1.27	1.27	$\bar{2}$20	w
20	1.24	1.24	01$\bar{3}$	w
21	1.22	1.22	$\bar{2}$21,311	w
22	1.21	1.21	11$\bar{3}$	m

* attributed to transition phase

TABLE 6 (continued)

Line	Observed d(Å)	Calculated d(Å)	h k l	Observed relative intensity
23	1.18	1.18	11$\bar{3}$	m
24	1.17	1.17	113,0$\bar{2}$2,203	w
25	1.11	1.11	$\bar{2}$13	w
26	1.10	1.10	$\bar{4}$01,$\bar{4}$10, $\bar{3}$20,2$\bar{1}$3	mw
27	1.09	1.09	31$\bar{2}$	w
28	1.03	1.03	004	mw
29	1.01	1.01	303	w
30	1.00	1.00	$\bar{1}$04,22$\bar{2}$	mw
31	0.992	0.992	402	w
32	0.895	0.895	$\bar{5}$01	mw
33	0.880	0.884	131,$\bar{5}$11,522	mw
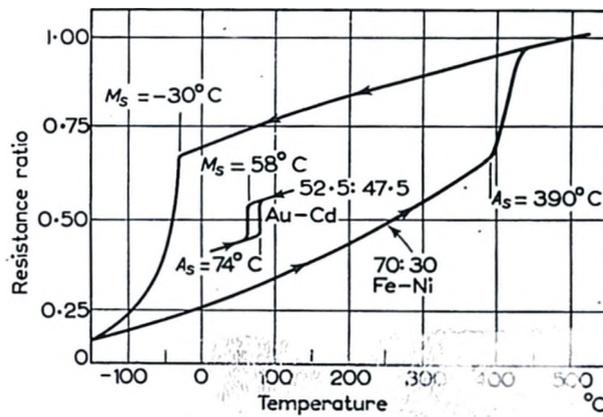
Fig. 1.   Electrical resistance changes during the heating and
          cooling of an iron-nickel and a gold-cadmium alloy,
          illustrating the hysteresis between the martensitic
          reaction on cooling and the reverse transformation
          on heating (after Kaufman and Cohen [12]).
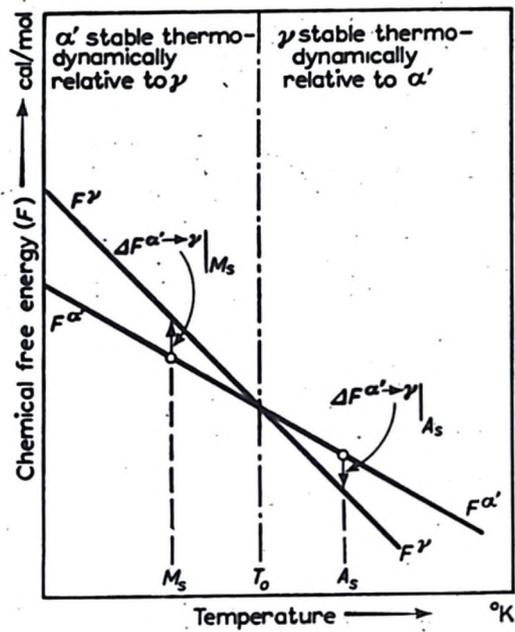
Fig. 2. Schematic representation of $F^{\alpha'}$ and F^{γ} as a function of temperature for an iron-base alloy. (after Kaufman and Cohen [12])

Volume $\cong \pi r^2 c$
Surface area $\cong 2\pi r^2$

2c

Habit plane
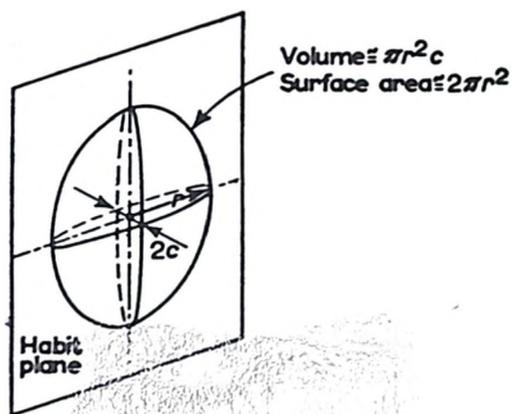
Fig. 3.   Schematic drawing of a martensite embryo (after Kaufman and Cohen (12))
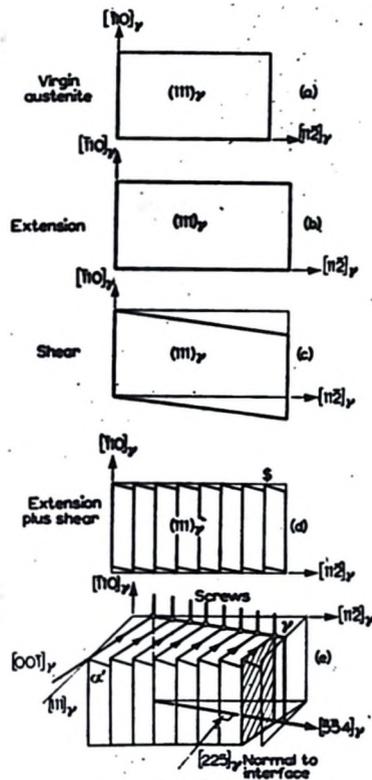
Fig. 4.   Frank's model of the austenite-martensite interface in an iron-base alloy (after Kaufman and Cohen [12])

$$d = \frac{6a_y}{\sqrt{2}} \; \frac{1}{\cos\eta} = 17\cdot 8 \; \overset{\circ}{A}$$

$$b = \frac{a_y}{2\sqrt{2}}$$

$\eta = x$ between $[55\bar{4}]$ and $[1\bar{1}0]$

$[1\bar{1}0]_y$

$2c$

Negative screw

S

d

$2r$

$[55\bar{4}]$

$[225]_y$

Positive screw

Dislocation loops
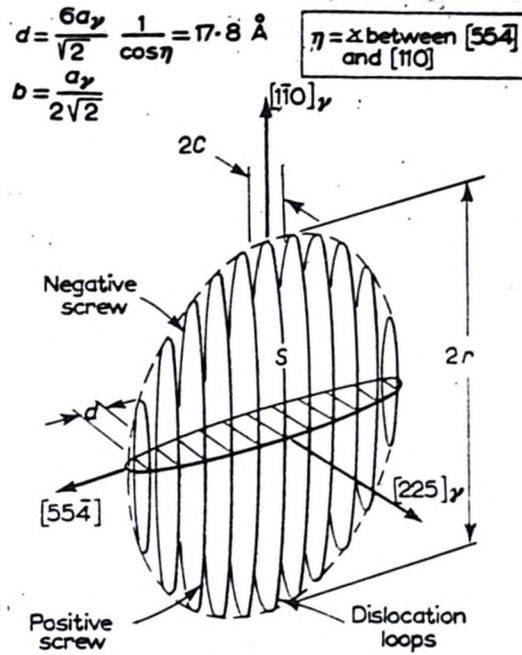
Fig. 5.   Knapp and Dehlinger's model of the martensite embryo in an iron-base alloy (after Kaufman and Cohen [12])
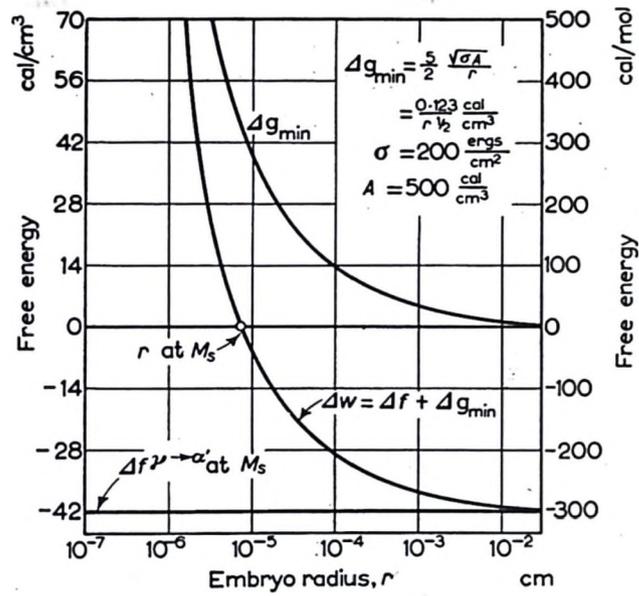
Fig. 6. Effect of embryo size on the restraining force Δg_{min} and the net driving force Δw according to Knapp and Dehlinger (after Kaufman and Cohen [12])
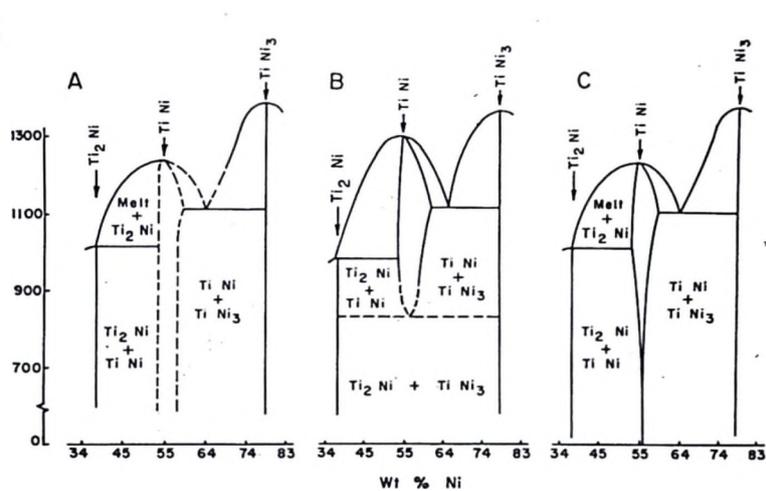
Fig. 7. The Ti-Ni equilibrium phase diagram showing three versions
of the TiNi phase boundary according to: (A) Margolin,
Ence and Nielsen [4]; (B) Duwez and Taylor [2]; (C) Purdy
and Parr [6] (after Buehler and Wiley [7])
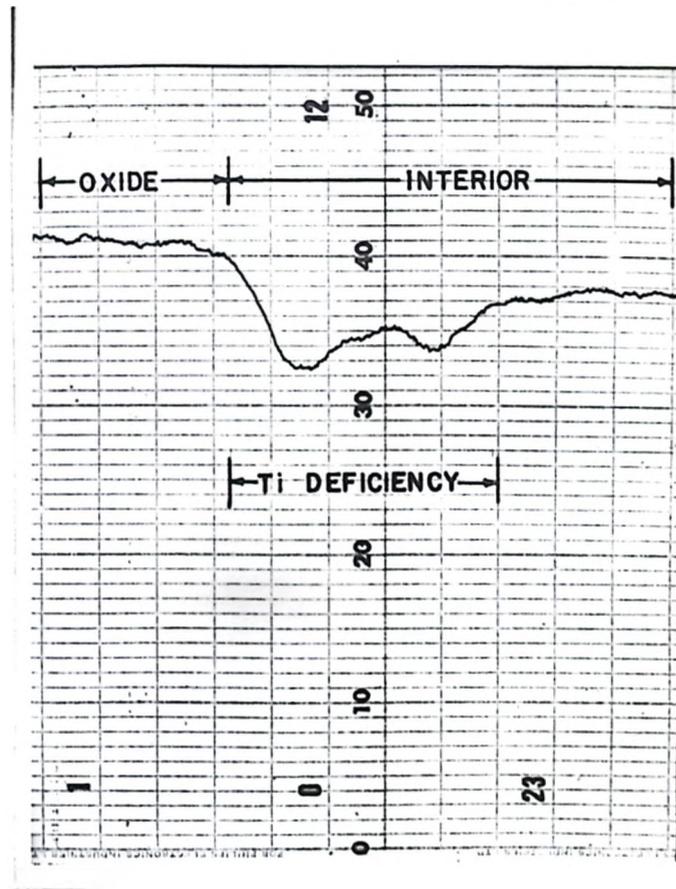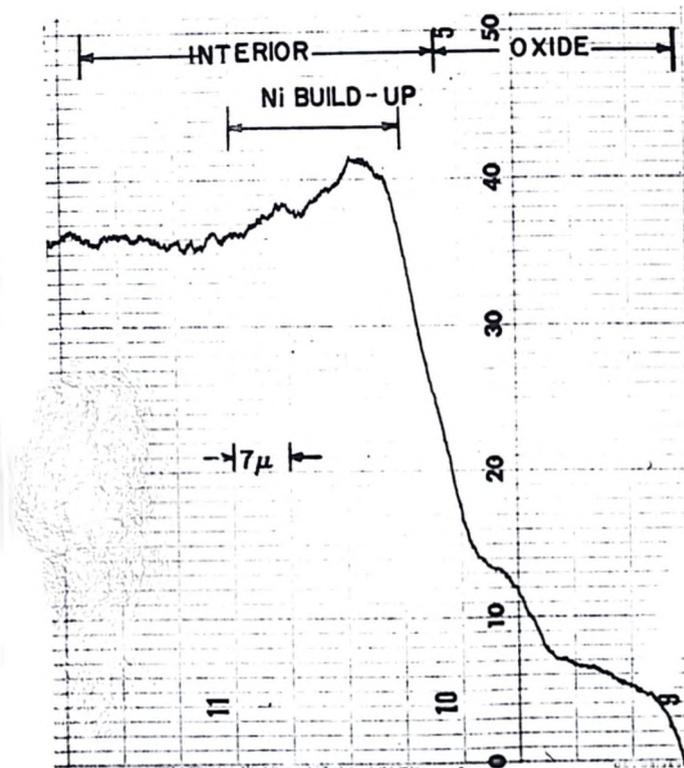
Fig. 8   Microprobe traces across the oxide metal interface of an oxidized wedge-sectioned single phase (51% Ni) alloy showing a nickel build up and titanium deficiency below the oxide.
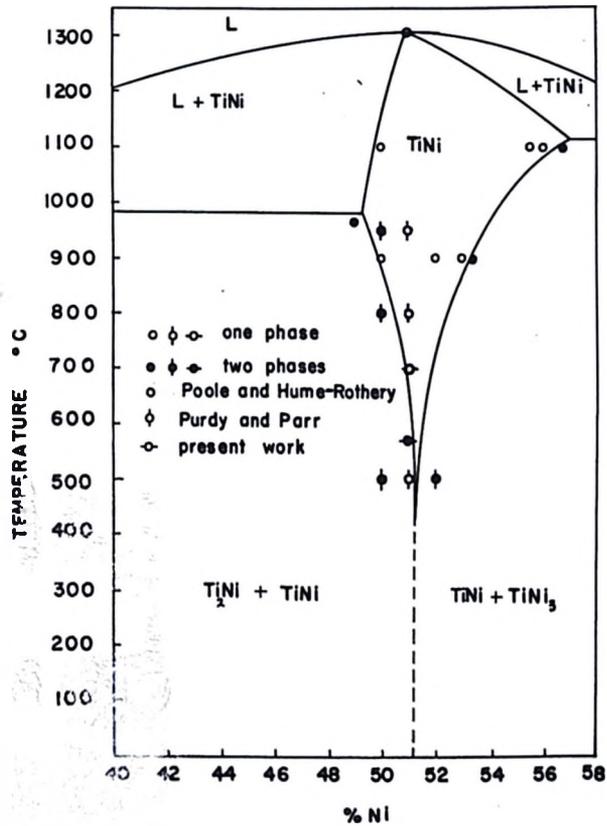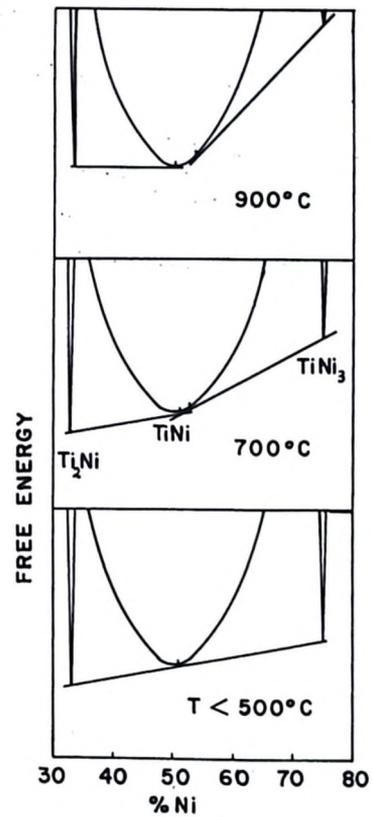
Fig. 9   (a) Equilibrium phase diagram in the region of TiNi.

(b) Schematic free energy diagrams drawn corresponding to the decreasing composition range of TiNi and suggesting the possibility of a eutectoidal decomposition at some temperature below 500°C.

Fig. 10(a) Single phase material (51% Ni) annealed at 700°C for
15 minutes (sample H-700-1) X 25000
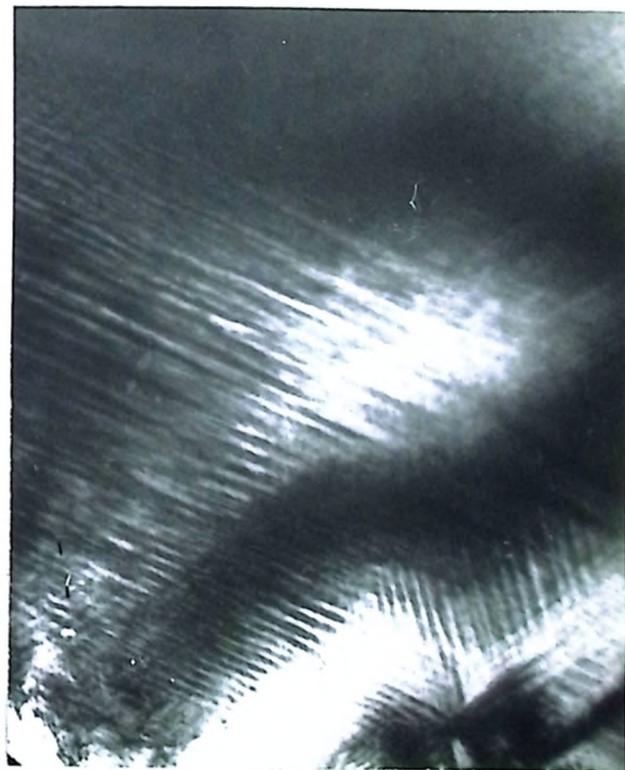
Fig. 10(b) Stripe contrast found in 51% Ni alloy annealed at 700°C for
50 minutes to 5385 minutes.

x 20000   x 30000
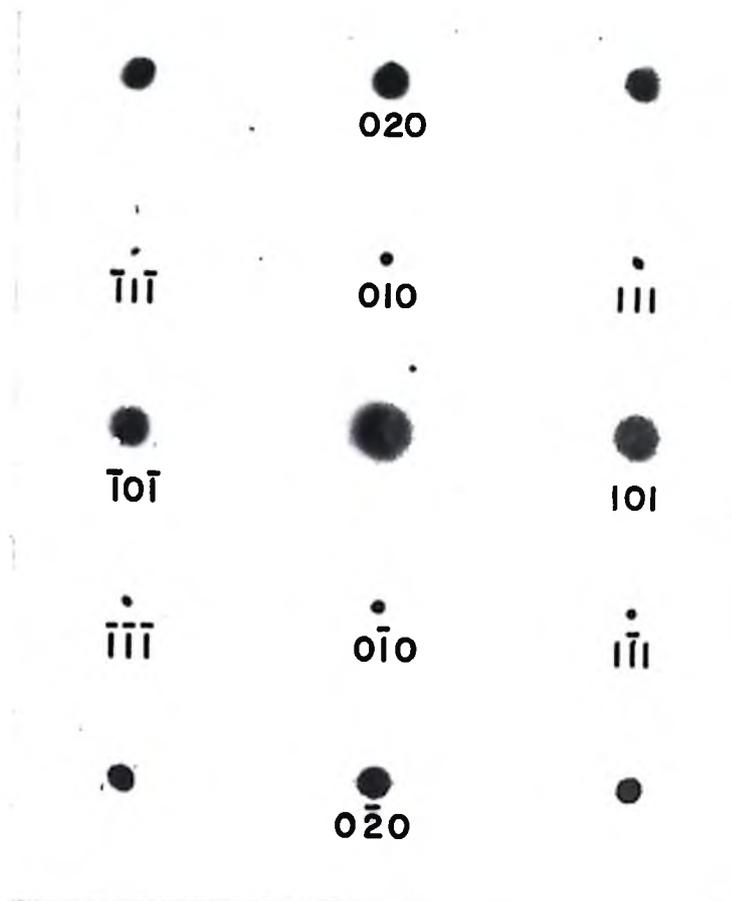
Fig. 10(c) Indexed electron diffraction pattern (typical of the H-700 series) very near to the Bragg condition showing CsCl superlattice spots.

Fig. 10(d) Electron diffraction pattern (typical of the H-700
series) taken at some deviation from the Bragg
condition showing diffuse diffraction maxima in
addition to the body-centered-cubic CsCl pattern.

Fig. 11(a) 51% Ni alloy annealed at 700°C for 5385 minutes
followed by 460 minutes at 500°C (sample R-500-2)
showing coherent precipitates which are presumed
to be Ti$_2$Ni   X 30000

Fig. 11(b) Electron diffraction pattern showing diffraction
streaks due to the coherent precipitation of a
second phase (taken from II-500-2).

Fig. 11(c) Electron diffraction patterns showing weak super
lattice spots (in addition to strong b.c.c. $a_0 = 3.01$ Å
spots) which can be indexed on the basis of a 9.03 Å
simple cube (taken from II-500-3).
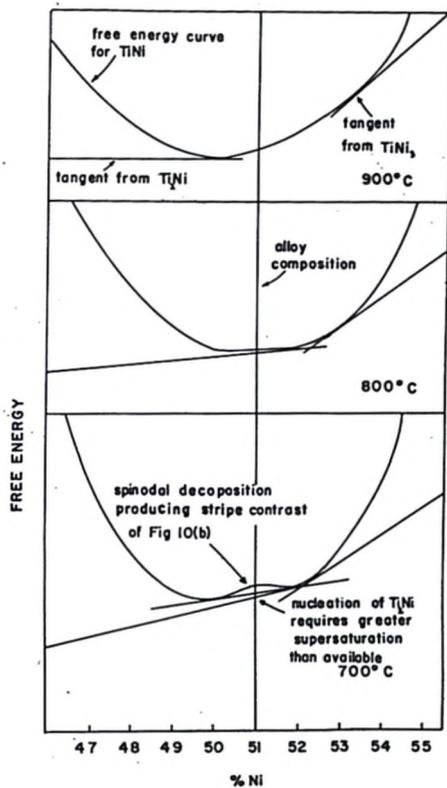
Fig. 12. Schematic free energy-composition curves showing the development of the instability in TiNi which results in a spinodal decomposition at 700°C.
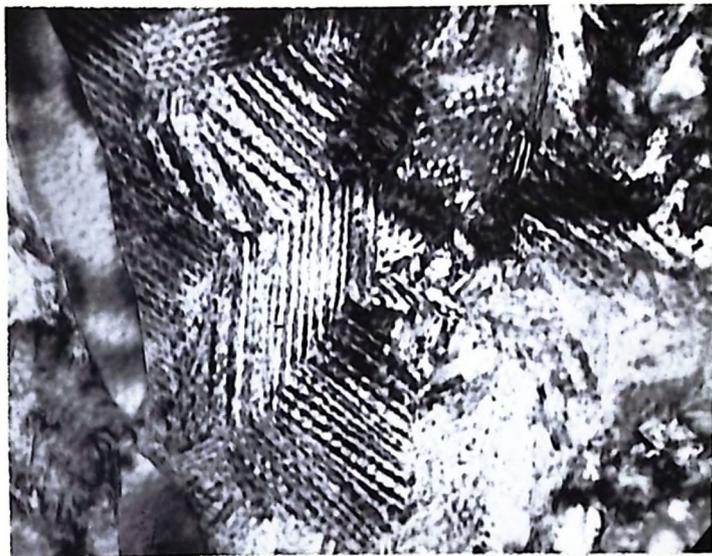
Fig. 13. Microstructure observed in H-500-4 after the thin film
specimen was allowed to stand at room temperature for
several weeks.   X 63000
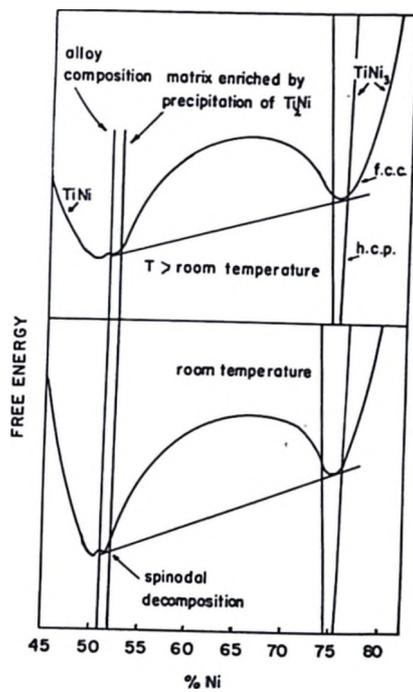
Fig. 14. Schematic free energy-composition diagrams showing the development of the conditions that lead to the postulated spinodol decomposition at room temperature.
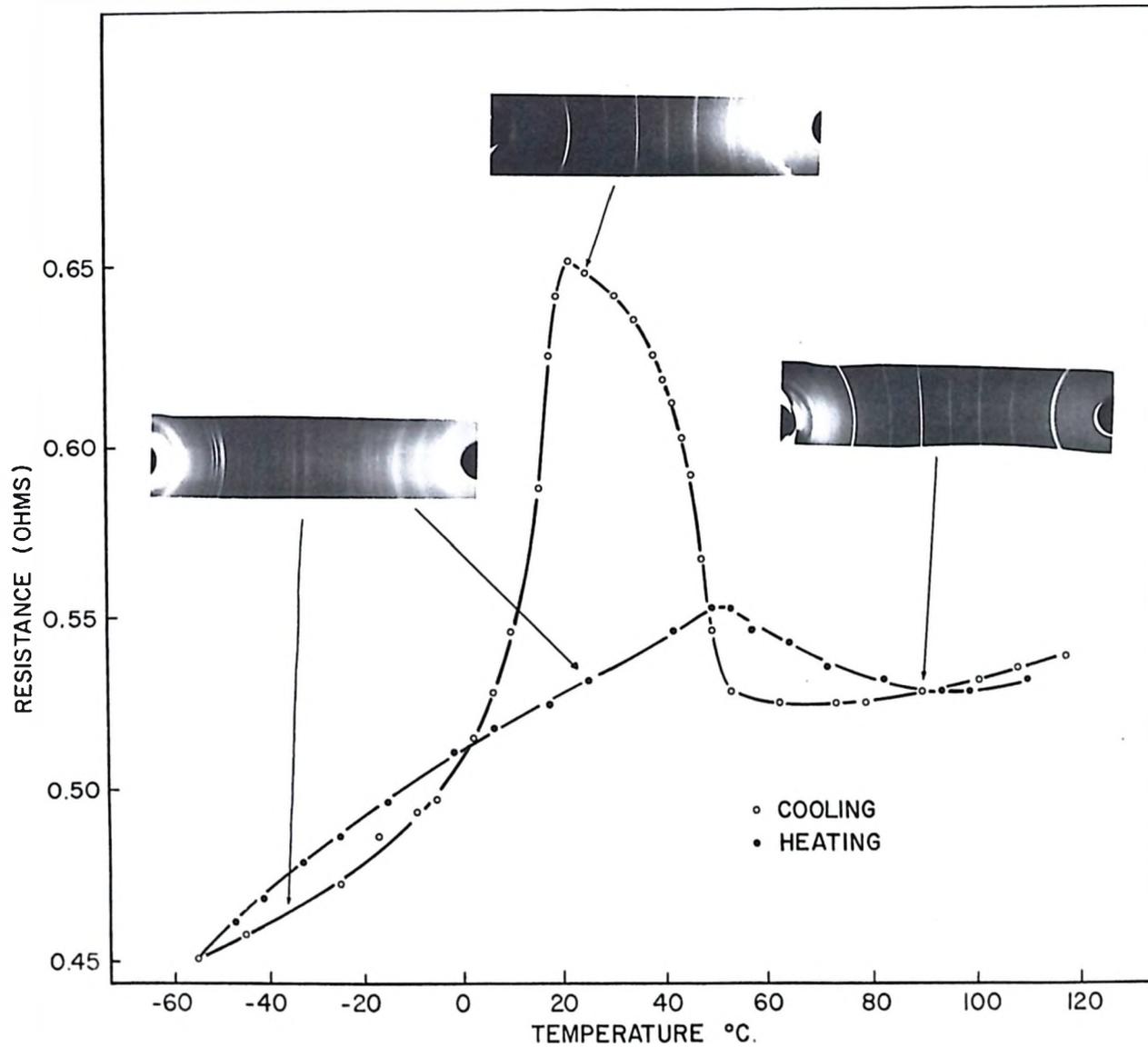
Fig. 15   Resistance vs. temperature during the heating and cooling of a 50% Ni alloy with superimposed powder patterns.
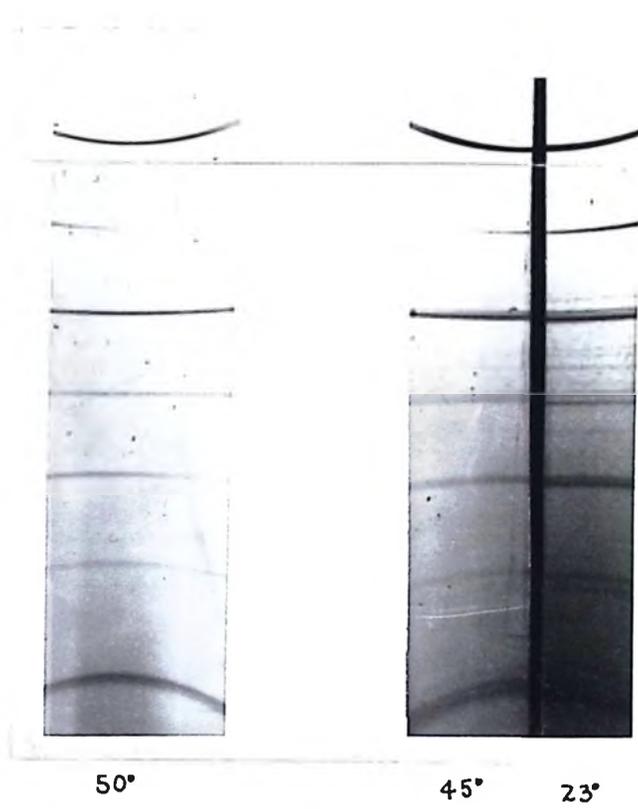
Fig. 16. A sequence of X-ray diffraction powder photographs of
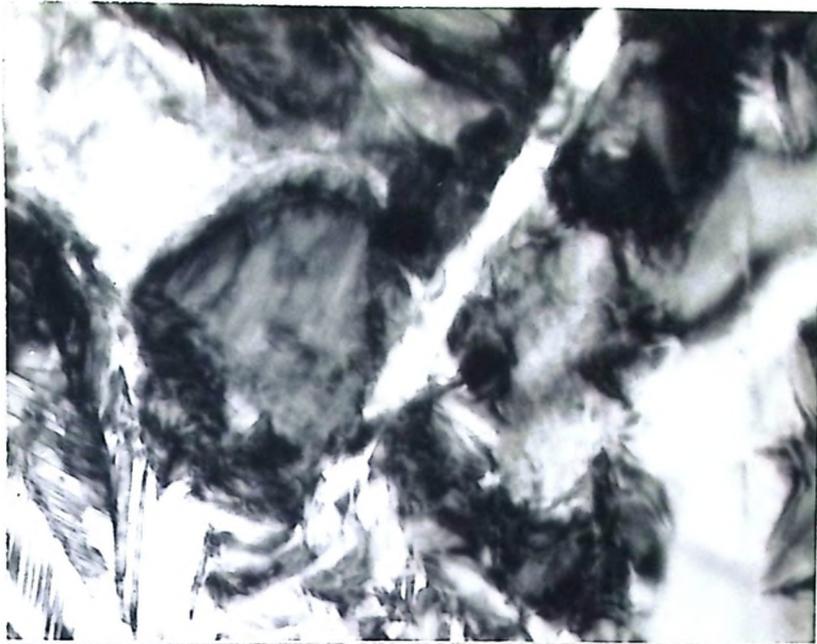the transition phase taken (from left to right) at 50°C,
45°C and 23°C.

Fig. 17(a) Electron micrograph showing a Ti₂Ni precipitate and some twinned martensitic phase in a matrix of transition phase.   X 94000

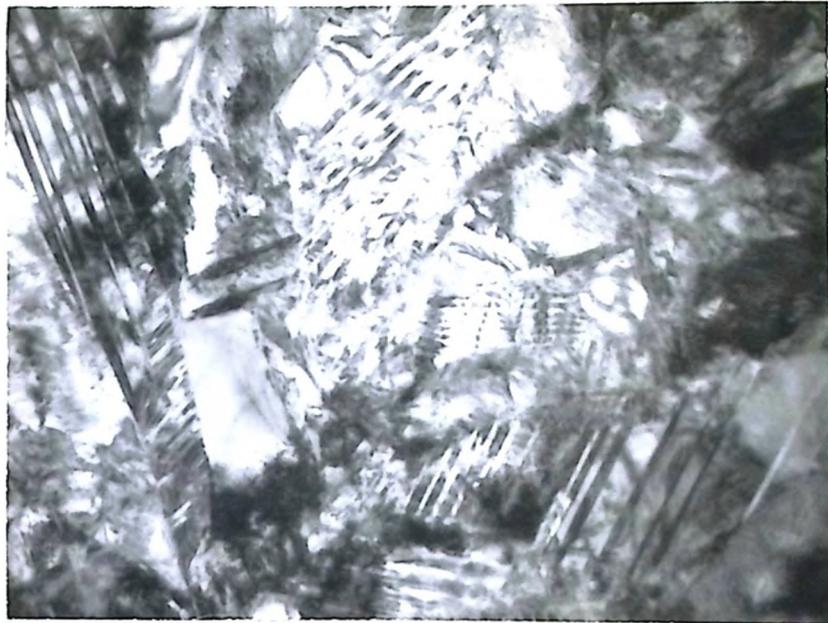Fig. 17(b) Electron diffraction pattern of the transition phase.

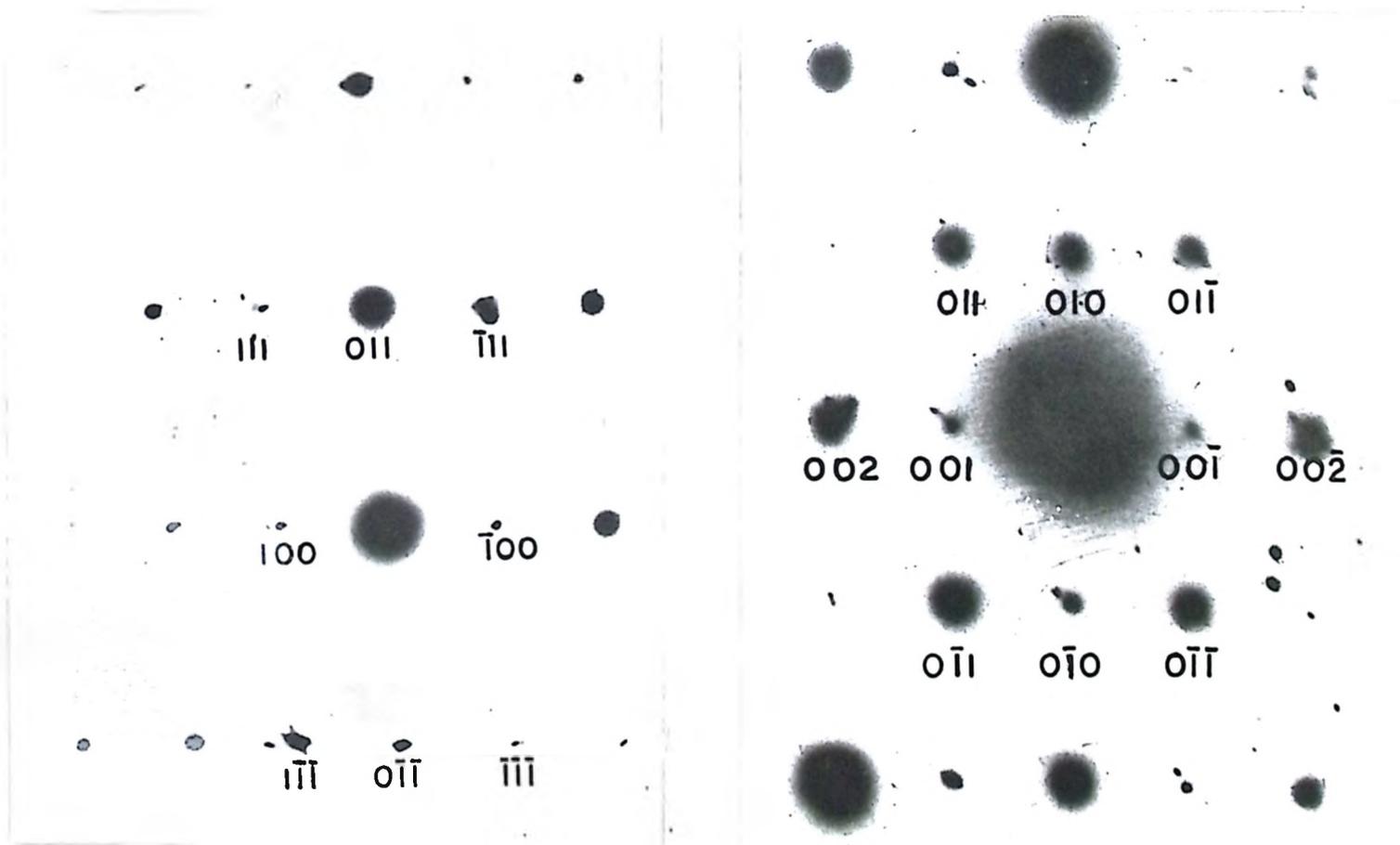Fig. 18(a) Electron micrograph of the martensitic phase.   X 30000

Fig. 18(b)   Indexed electron diffraction patterns of the martensitic phase.

Fig. 18(c)   One of the more complex electron diffraction patterns
obtained from the martensitic phase.

(a)   (b)

Fig. 19   Electron diffraction patterns showing the orientation
relationship between adjacent areas of (a) parent phase,
and (b) martensitic phase.